Quadruple Langmuir Probe Measurements of a Hall Effect Thruster Plume

Reed Keefer Thompson

A thesis
submitted in partial fulfillment of the
requirements for the degree of

Master of Science in Aeronautics and Astronautics

University of Washington

2022

Reading Committee:

Justin Little, Chair

Uri Shumlak

Program Authorized to Offer Degree:
Aeronautics and Astronautics

University of Washington

Abstract

Quadruple Langmuir Probe Measurements of a Hall Effect Thruster Plume

Reed Keefer Thompson

Chair of the Supervisory Committee:
Justin Little
Aeronautics and Astronautics

Measuring time-dependent plasma parameters requires a diagnostic capable of making instantaneous measurements. A quadruple Langmuir probe measures the instantaneous electron temperature, electron density, and ion velocity. In this thesis, a quadruple Langmuir probe was designed, manufactured, and utilized to characterize the breathing mode of a Hall Effect Thruster. This quadruple Langmuir probe has a probe radius of 0.117 cm and collects current with graphite electrodes. An applied potential of approximately 27 V was applied to the ion saturation current collecting parallel and perpendicular probes. A measurement of the breathing mode was successfully taken for a Hall thruster operating with a discharge voltage of 250 V. The frequency of the breathing mode was estimated to be 28.4 kHz. The electron temperature varied between 1 and 3.4 eV for one breathing mode cycle. The electron density was measured on the order of 10^{17} m^{-3}. Thin-sheath quadruple Langmuir probe theory was used, but results indicated that transitional sheath theory should be applied. Using the collected data, the average Mach number and ion velocity was calculated at 10.9 and 14 km/s, respectively. The plasma potential was calculated to have a mean value of 15.3 V, estimated from the electron temperature. Trends of time averaged plasma parameters were also compared with the Hall thruster's discharge voltage. Quadruple Langmuir probe measurements of a Hall thruster breathing mode have been presented.

TABLE OF CONTENTS

LIST OF FIGURES

LIST OF TABLES

ACKNOWLEDGMENTS

This work would have not been possible if not for the support of my advisor, Dr. Justin Little. He first introduced me to electric propulsion in 2018, where he taught me about vacuum systems, pumps, and electric thrusters. After taking his class, he gave me an opportunity to conduct research into magnetic shielding for Hall thrusters while I was pursuing my undergraduate degree. I continued working with him as a masters student where I would begin the work presented in this thesis. While knowing him, Dr. Little has always provided support towards my continued study of electric propulsion. I am grateful for everything he has done for me.

Next I would like to thank Dr. Uri Shumlak. Professor Shumlak has taught me a great deal about plasma physics. My favorite class of his was plasma diagnostics where he suffered many long hours of me asking silly questions. He has been most gracious to provide his support as I look for my place in the field of electric propulsion.

I would also like to thank everyone studying plasmas in the department. We have spent many hours together in the lab and studying for classes. To me you have provided a sense of community and I have enjoyed your friendship.

I would like to thank Aqil Khairi, Peter Thoreau, Landon Bevier, Maria Politi, Arvindh Sharma, and Sari Barczay for lending your support during my time in the masters program. May you all be successful in your future endeavors.

Finally, I would like to thank my family and friends. You have provided the most support throughout my academic career. Thank you to my mother and father for providing me with a life where I can pursue my dreams. I would like to thank my brother who reminds me that

it is good to take a break every now and again and have some fun. I would like to thank all the friends I have made along the way, who have provided me with many fond memories to look back on and cherish. I hope you all have the opportunity to pursue your dreams. Thank you.

Nomenclature

ΔW	uncertainty of variable W
ϵ_0	permittivity of free space
λ_D	Debye length
λ_{ee}	electron-electron collisional mean free path
λ_{ei}	electron-ion collisional mean free path
λ_{en}	electron-neutral collisional mean free path
λ_{ii}	ion-ion collisional mean free path
λ_{in}	ion-neutral collisional mean free path
λ_{nn}	neutral-neutral collisional mean free path
ϕ	electron charge to electron temperature ratio
σ	collisional cross-section
τ_L	end effect parameter
B	magnetic field
$\vec{E}$	electric field

A	current collection area
A_e	electron current collection area
A_i	ion current collection area
$A_\perp$	current collection area of perpendicular probe
c_m	most probable thermal ion speed
d_s	sheath thickness
e	electron charge
I_l	collected current by probe l
$I_\perp$	collected current by perpendicular probe
I_{sp}	specific impulse
J_e	electron saturation current density
j_e	electron current density
J_i	ion saturation current density
j_i	ion current density
k	Boltzmann Constant
L_p	probe length
m_e	electron mass

M_i	ion Mach number
m_i	ion mass
n_e	electron density
P_l	probe l, for l = 1, 2, 3, 4
r_p	probe radius
$T_{e,i}$	electron or ion temperature
u_i	ion velocity
V_f	floating potential
V_l	voltage of probe l
V_p	plasma potential
V_{dl}	voltage difference of Probe l and Probe 1
V_o	limit of sheath formation

Chapter 1
INTRODUCTION

Studying the natural sciences allows engineers to develop technology to accomplish goals they determine as imperative. Quantifying natural phenomena through theory sets rules and guidelines for engineers to follow and design technology to make life easier for everyday people. To measure natural phenomena an engineer relies on previously established theory and techniques to model the behavior and gain insight of the dynamics of the devices they create. This thesis aims to measure the plasma parameters in the plume of ACME Hall thruster via the SPACE lab quadruple Langmuir probe.

Satellites carry important tools to communicate, measure geophysical data, and provide internet. However, satellites are not naturally occurring objects and they require engineers to design and send them to orbit. Chemical propulsion systems send satellites to orbit and electric propulsive systems keep them there. Both propulsion systems operates under Newton's third law, mass must be expelled from the system in a controlled manner to send it in the opposite direction. The first satellite, Sputnik, launched into orbit by the Soviet Union in 1961 [24] using chemical rockets, a concept known for centuries. Ancient Chinese civilizations invented fireworks, the first form of chemical rockets.

While chemical rockets are still required today to escape Earth's gravity, electric propulsion devices have been developed, tested, and deployed in orbit because of their advantages

over chemical propulsion. The most important one is their capability of reaching higher specific impulses, I_{sp}. Specific impulse compares the amount of thrust a rocket motor generates to the rate at which fuel is used. Specific impulse is a mass utilization efficiency measurement. Electric propulsion provides approximately an order of magnitude higher I_{sp} than chemical rockets. For example, Hall thrusters provide a specific impulse from 1220 s to 2150 s while chemical rockets provide only 200 s to 468 s of specific impulse [30]. Electric propulsion devices also have lower mass requirements, have longer operational lifetimes, and achieve higher exhaust velocities when compared to chemical propulsion systems.

The Hall effect thruster is one type of electric propulsion device. The first Hall thruster, or stationary plasma thruster, was designed and manufactured in 1964 at the Kurchatov Institute of Atomic Energy [26]. Hall thrusters have flown on many Russian, European, and American missions, mainly for orbit raising and station keeping [30]. Hall thrusters provide thrust by accelerating ionized fuel by an axial electric field between the anode in an annular channel and the cathode positioned outside the acceleration channel. To create ions, gaseous fuel, most commonly Xenon, enters the acceleration channel of a Hall thruster from the anode and is ionized by collisions with electrons that have been supplied by the cathode. The cathode supplies the electrons using thermionic emission to neutralize the plume and ionize the fuel. Electrons are attracted into the channel by the axial electric field to the anode, but due to the magnetic field created by two separate electromagnets the electrons become trapped inside the channel of the Hall thruster. The $\vec{E} \times \vec{B}$ force that traps the electrons is called the Hall effect current. These trapped electrons are the source of ion creation. Ions are accelerated away from the thruster and pull electrons from the cathode to maintain charge neutrality of the system [10].

The first Hall thruster was not utilized in space until 1971, on one of the Meteor meteo-

rological satellites [26]. Outside the Soviet Union, the first implementation of a Hall thruster on mission to space occurred in 1998 on a U.S. government experimental spacecraft [14]. Hall thrusters provide a very small amount of thrust so their primary purpose is to maintain or change a satellites orbit. To change a satellites orbit significantly, Hall thrusters must operate for extended periods of time. Hall thruster lifetimes are characterized by tests that can last up to ten-thousand hours. Another first for Hall thruster technology occurred when the European Space Agency sent a Hall thruster on the SMART-1 mini-satellite in orbit around the moon [19]. This technology has become so reliable that it has been deployed around a different celestial body. However, before an electric propulsion system is mission-ready, its performance needs to be characterized using established diagnostic methods. Measurements of plasma parameters in the plume of the electric propulsion device can be one way to characterize performance.

Plasma parameters in Hall Thruster plumes have been characterized by many different methods both using perturbing and non-perturbing techniques. Electrostatic probes are a common way to measure plasma parameters and single Langmuir probes have been used to measure plasmas since they were developed in 1926 by H. M. Mott-Smith and Irving Langmuir [27]. Single Langmuir probes measure the electron temperature and density by sweeping the applied voltage and measuring the collected current. However, having to sweep the voltage prohibits the probe from measuring phenomena that occur on smaller time-scales than the sweep. Analyzing single Langmuir probe data can be quite time intensive. However, previous work has found that by adding more probe tips, instantaneous measurements of electron temperature and density can be made and the analysis can be done quicker. Chen and Sekiguchi developed the triple Langmuir probe [6]. Burton improved on their design with the first application of the quadruple Langmuir probe [5].

1.1 Quadruple Langmuir Probes in Practice

Quadruple Langmuir probes (QLP) measure the instantaneous electron temperature, density, and ion speed. Thus QLPs are an excellent technique to characterize the plume of electric propulsion devices like Hall thrusters. QLPs are a combination of a triple Langmuir probe and a crossed electrostatic probe. Chen developed the triple probe to make instantaneous measurements of the electron temperature and density [6]. The crossed probe was first used in an experiment by Johnson and Murphree as method to measure the ion speed in moving plasmas. The crossed probe current collection theory was developed by Kanal [17]. Combining the two techniques allowed Burton to create one diagnostic and study these plasma parameters in the plume of a magnetoplasmadynamic thruster [5]. Since then, QLPs have been used to study plumes of arcjets and PPTs [4][8][33].

While quadruple Langmuir probes (QLP) have yet to be used to characterize Hall thruster plumes, they have been successfully used to make measurements in other electric thruster plumes. Burton was first to apply the QLP technique in 1993, to study a pulsed Magneto-Plasma Dynamic thruster [5]. Bufton studied under Burton and wrote a dissertation on plume measurements of a hydrazine arcjet using the QLP technique [4]. The QLP technique was also applied to the Plasmoid Thruster Experiment studied by Koelfgen [18]. Work done by Gatsonis and Zwahlen, developed a new operation mode denoted the current mode for the QLP operation while studying the plume of a PPT [8][33].

The first measurements made using a QLP were on a pulsed 1.5 MW Magneto-Plasma Dynamic thruster. The thruster had a 9 cm long hollow cylindrical copper anode and tungsten cathode at its center while argon was supplied at the base in between the anode and cathode [5]. The QLP was used to measure the plume at 3 cm to 25 cm from the thruster exit consisted of four 0.25 mm diameter and 5 mm long tungsten probe tips, three of which

were parallel to plasma flow and one was perpendicular. Using different fixed biases on nearly every probe, Burton was able to make an instantaneous measurement of the electron temperature, electron density, and ion speed for a single 1.1 ms pulse of current. As the probe was positioned closer to the thruster, the temperature, density, and speed varied from 1.5-8 eV, 1.2-4.8$\times 10^{19}$ m^{-3}, and 1.8-0.7$\times 10^{4}$ m/s, respectively. The density had the highest error, but the average percentage of error over all parameters was 29%.

Bufton used the QLP technique to quantify plasma parameters in the plume of a 1 kW Hydrazine arcjet, and this work was for their dissertation under Burton. In this study the QLP had 0.25 mm diameter tungsten electrodes [4]. The parallel flow electrodes had a length of 2.5 mm and the perpendicular probe had a length of 2 mm. This work not only expanded the QLP theory to find the same plasma parameters for multiple ion species, but also was able to measure radial gradients of those parameters in the plume.

1.2 Hall Effect Thrusters and TLP

After Chen published the Triple Langmuir Probe (TLP) method in 1964, many experiments have since been published studying Hall effect thrusters using this technique. Giannetti studied breathing mode oscillations in Hall thrusters using a moving TLP [10]. Li used a TLP to characterize the plume plasma parameters from a microwave generated plasma accelerated through a linear Hall current plasma accelerator [22]. Beal has published two papers that used the TLP technique to study Hall thruster clusters [1][3]. A summary is provided for each experiment mentioned using TLPs.

Hall thrusters have many unsteady modes that affect their performance, but one of the unstable low frequency modes that often appears is known as the breathing mode [10]. Giannetti conducted this study in 2020, aiming to measure the breathing mode from the plume

to the channel exit and into the discharge channel. This was accomplished by oscillating the axial location of the probe in the discharge channel to limit the amount of time spent in dense plasma. Since the time scale of the probes motion was slower than breathing mode oscillation, Giannetti presented features of the plasma oscillations by taking instantaneous measurements of plasma parameters using the TLP technique. Five cycles of the breathing mode were shown in a spatial-temporal map of the electron temperature, density, and plasma potential. All plasma parameters were coupled to the discharge current oscillations thus defining the breathing mode.

TLPs have also been used to study microwave-generated plasmas in a linear Hall current plasma accelerator [22]. In 2003, Li published their dissertation on the acceleration of plasma due to the Hall effect. While this study was not conducted on a traditional Hall thruster, part of their analysis used a TLP to characterize the plume accelerated by a Hall current. The linear hall current plasma accelerator was positioned such that the plasma jet from the microwave thruster fed directly into the accelerator's channel. Li used the TLP to measure the electron temperature and density to work out the electrical conductivity, Hall parameter, and ionization fraction of the plasma leaving the accelerator. Measurements from the TLP found that over time the electron density and temperature were continuous, but did not operate in a steady state. The results showed that the plume lacked symmetry as peak plasma parameters were not aligned with the geometric center of the accelerator.

Hall thruster clusters are a method of scaling up power for a propulsion system without having to create a single high powered thrust device. This offers advantages such as redundancy and thrust throttling [1]. However, this also introduces the possibility of plume interactions that inhibit thruster operation. Beal has published two studies on Hall thruster clusters and their plume characterization using a TLP [1][3]. Both studies use four Busek

200-watt Hall thrusters equally spaced. Each study uses the TLP to create spatial maps of the electron density, temperature, and plasma potential. Beal's first study in 2002, made preliminary spatial measurements along the cluster centerline and the centerline of thruster pairs to characterize the plasma parameters in the axial direction [1]. Beal's second study in 2004, made these spatial measurements again, but this time to characterize the plasma parameters in the cluster plume based on how many thruster were in operation [3].

TLPs have been used to characterize plasma plumes of thrusters driven by Hall currents. Since the instantaneous measurement of electron temperature and electron density is possible, transient and oscillatory phenomena reliant on these plasma parameters can be studied directly. The measured parameters can be used to make deductions about other aspects of the plasma, like the Hall parameter and ionization fraction. It is possible to use this technique to make spatial maps of these plasma parameters in plumes of Hall thrusters. A quadruple Langmuir probe (QLP) is a combination of a TLP and a crossed electrostatic probe, therefore measurements in Hall thruster plumes using a QLP should be possible.

1.3 Objectives and Approaches

Using a Quadruple Langmuir Probe (QLP) to measure plasma parameters in a Hall thruster plume has not yet been achomplished. Triple Langmuir probes (TLP) have been used to map trends in Hall thruster plumes and in the acceleration channel [10][12]. One experiment used a replica of a QLP to measure the erosion of its protective outer ceramic wall due to $\vec{E} \times \vec{B}$ current in the acceleration channel of a Hall thruster, but the QLP was not operational[12]. A QLP has now been used to characterize the plasma parameters in the plume of the ACME Hall thruster developed in SPACE Lab at the University of Washington.

This thesis is focused on the development and testing of a QLP to measure the electron temperature, density, and ion speed in the plume of the ACME hall thruster. The ACME Hall thruster is magnetically shielded with a nominal power rating of 500 W and operates using Xenon [31][32]. This work provides the first plume measurements of a Hall Thruster using the QLP technique. Moreover, this is the largest QLP relative to other experiments that use this technique. The QLP design presented here also uses graphite tips to record measurements. Here are the objectives of the thesis:

- Design a QLP with a capability to measure the electron temperature, electron density, and ion speed for reactive propellant by-products. Able to measure these plasma parameters in future thrusters that use water as propellant. Base design off of preliminary measurements of the plasma parameters from Electron Cyclotron Resonance thruster.

- Construct the QLP using readily available and cost-effective materials. Create and execute procedures for in house machining of critical parts for QLP construction.

- Develop procedures for data collection under Hall thruster steady state operating conditions using guidelines from previous work [4][33].

- Take measurements of plasma parameters of Hall thruster operating at different conditions of discharge voltage, anode flow rate, and cathode flow rate.

- Conduct an analysis of the data by writing an algorithm to simultaneously solve Burton's [5] equations and measurement uncertainty analysis described by Gatsonis [8]. Determine if the Hall thruster breathing mode can be measured.

Chapter 2 delves into the methods conducted in this thesis; including the design of the QLP, the experimental setup and the procedures of data collection. Chapter 3 will discuss the results of the experiment and their fidelity in accordance with the manner that they

were produced. Finally, chapter 4 provides the conclusions related to the work offered in this thesis and recommendations for the continuation and improvements of the QLP method.

Chapter 2

METHODS

Measurements of the ACME Hall thruster were taken in the Space Test Facility (STF) vacuum chamber using a quadruple Langmuir probe (QLP). The STF is located in Seattle, Washington at the University of Washington's Space Propulsion and Advanced Concepts Engineering laboratory, also known as SPACE lab. Within the STF, the QLP was positioned upon the dual axial translation stage and aligned to the chamber and Hall thruster centerline. This chapter will discuss in more detail about the facilities, the QLP method, and the procedures used in operation.

2.1 Facilities and Hall Thruster

SPACE lab has been in operations since 2018. SPACE lab is supported by the Air Force Office of Scientific Research, Air Force Research Laboratory, National Science Foundation, National Aeronautics and Space Administration and the Joint Center for Aerospace Technology Innovation. The largest chamber, the STF, was used to take QLP measurements of the Hall thruster. The ACME Hall thruster was attached to an inverted pendulum thrust stand centered in front of the STF axis door. ACME is a magnetically shielded 500 W class Hall thruster. This section will describe each system in greater detail.

2.1.1 Vacuum Chamber - STF

The SPACE Lab, Space Test Facility (STF) vacuum chamber consists of a 1.4 m diameter spherical test section and a 1 m diameter by 1.7 m long cylindrical extension. The spherical chamber and the extension were both made of stainless steel. On the spherical test section reside 108 ports to accommodate multiple diagnostics. Unused ports were covered in aluminum foil. Inside the spherical test section, diagnostics were installed on two stacked single axis translation stages to provide two-dimensional translation. Each translation stage operate with stepper motors which aligned the QLP along the Hall thruster centerline and positioned approximately 6 Hall thruster diameters from the exit plane of the thruster. The inverted pendulum thrust stand was locked onto a dual rail system, isolated from the moving translation stage. This allows for easy removal and installation of the thrust stand. The thrust stand was positioned in front of the 89 cm diameter main access door of the spherical test chamber.

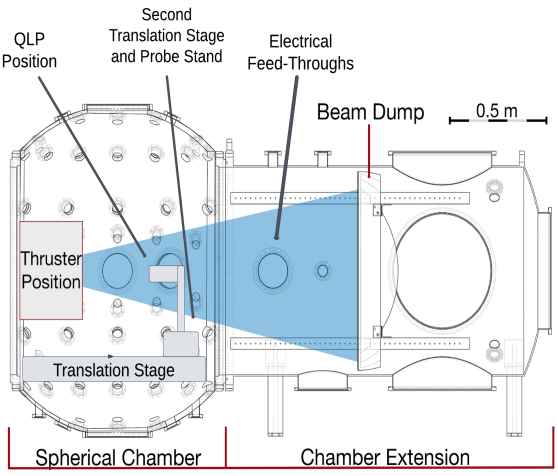

Figure 2.1: Diagram of the STF vacuum chamber with approximate probe location.

Directly opposite of the Hall thruster, downstream of the plume, the cylindrical extension was attached to the spherical test chamber. The chamber extension contains multiple pumps, electrical connection feed-throughs, and the beam dump. The STF has the capacity for three Sumitomo cryopumps, but only utilizes two for this test. Additionally, a Shimadzu turbopump and a roughing pump were operating during testing. Contributions from these pumps achieve a pumping rate of 25 kL/s of nitrogen, 70 kL/s of water vapor, and 12 kL/s of Xenon. The STF base pressure was 10^{-7} Torr. However, actual background pressure measured by an ion gauge calibrated for air, ranged from 1.2-1.6$\times 10^{-4}$ Torr. The ion gauge was positioned behind the thrust stand to avoid effects from the plume on measurements of pressure. The background pressure varied depending on the anode flow rate of Xenon.

In the cylindrical extension, twelve BNC electrical feed-throughs were available for in-vacuum diagnostics. Four of these feed-throughs were utilized by the QLP. The beam dump consisted of multiple graphite-covered aluminum plates angled at 45^o offset from the chamber axis. The beam dump protects the cryopumps from damage due to directed highly energetic ion flow. The beam dump was water cooled to prevent overheating from the ion beam.

2.1.2 Hall Thruster

The ACME Hall Thruster or Adaptive-field Central-cathode Magnetically-shielded Electric thruster received its name because of its capability to axially adjust the position of the outer walls of the acceleration channel relative to the centrally mounted cathode. Therefore, ACME is capable of changing the magnet topology of the shielding by adjusting the relative position of the electromagnets [31, 32]. ACME relied on two concentric electromagnets to generate the magnetic shielding. Between the two electromagnets and their Boron Nitride insulation is the acceleration channel. The mean diameter of the acceleration region was

5.7 cm [32]. Magnetically shielding reduces the amount of ion bombardment of the channel walls by limiting wall erosion which extends thruster operational lifetime. This is because electron motion is limited around magnetic field lines which run parallel to thruster walls in magnetically shielded configurations. Thus, ions can only approach the channel walls in a limited capacity because quasineutrality must be maintained. Within the inner magnet was the centrally mounted hollow cathode which emits electrons to maintain charge neutrality and ionize propellant. At the rear of the acceleration channel, the anode supplied 99.9999% pure Xenon gas and a positive bias of the system.

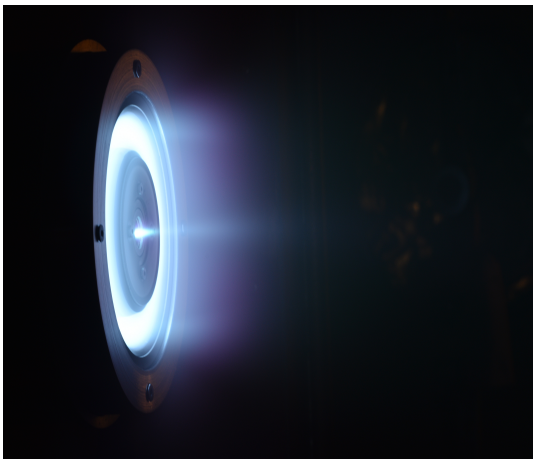

Figure 2.2: ACME on Xenon.

Hall thruster operating parameters included the discharge voltage, the anode flow rate, and cathode flow rate. The discharge voltage test points of the Hall thruster were 250 V, 300 V, 350 V, and 400 V. The anode flow rate of Xenon was tested at 14 sccm, 16 sccm, and 18 sccm. The cathode flow rate of Xenon was held at 3 sccm as other conditions were varied. However, additional tests were taken at a constant discharge voltage of 300 V, a constant anode flow rate of 16 sccm, and different cathode flow rates of 5 sccm, 8 sccm, 13 sccm, and

15 sccm. Throughout testing the inner and outer electromagnet amperage were kept at 13 A and 5 A, respectively. Thus maintaining a peak magnetic field strength of 181 G at the channel centerline. The inner and outer poles had no offset and the anode position did not change, thus a constant channel length to width ratio was maintained.

2.2 The Quadruple Langmuir Probe

An electrostatic probe originally developed by Burton [5], the quadruple Langmuir probe (QLP) utilizes four electrodes placed in a plasma to discern its natural parameters. The QLP combines a triple probe with a perpendicular probe. The QLP measures the instantaneous electron temperature, electron density, and ion speed. These parameters help characterize Hall thruster performance. In addition, the plasma potential was determined using these plasma parameters. This section will explain the underlying theory of quadruple Langmuir probes and its assumptions.

2.2.1 QLP Theory

QLP theory relies on the combination of two previously developed probes; the triple Langmuir probe developed by Chen and Sekiguchi [6] and the perpendicular electrostatic probe tested by Johnson and Murphee [15], but originally derived by Kanal [17]. The triple probe method determines the instantaneous electron temperature and density. The probe perpendicular to the flow collects current and is compared with the ion saturation current collected from a parallel probe to measure the instantaneous ion velocity.

Consider four probes with identical surface area, A. Three of the probes, P_1, P_2, and P_3, are parallel to the plasma flow. The last probe, P_4, is positioned perpendicular to the plasma

flow. Each probe has an applied potential that satisfies Equation. 2.1. P_3 and P_4 have the same sufficiently negative potential that collects ion saturation current. P_2 does not have an applied potential and was exposed to the plasma to acquire the floating potential. A voltage in between the floating potential and space/plasma potential is applied to P_1. P_1 collects a positive current equal to the collected current of P_3 and P_4, as seen in Equation 2.3. The electron temperature and density derivations done by Burton [5], require that the measured potentials were expressed as the potential difference between each probe relative to P_1, as defined by Equation 2.2.

$$V_3 = V_4 < V_2 = V_f < V_1 < V_p \tag{2.1}$$

$$\begin{cases} V_{d2} &= V_2 - V_1 \\ V_{d3} &= V_3 - V_1 \\ V_{d4} &= V_4 - V_1 \end{cases} \tag{2.2}$$

$$I_1 = |I_3| + |I_4| \tag{2.3}$$

Chen [6] and Burton [5] make the following assumptions such that the collected current can be written as seen in Equation 2.4. The assumptions made here will be discussed in more detail.

- The electrons in the plasma have a Maxwellian energy distribution.

- The ion sheath thickness around each probe is negligible compared to the probe radius and far smaller than the spacing between each probe to prohibit interactions between each probe.

- The mean free path of the electrons is much larger than the probe radius.

$$\begin{cases} -I_1 & = -AJ_e exp(-\phi V_1) + AJ_i(V_1) \\ I_2 & = -AJ_e exp(-\phi V_2) + AJ_i(V_2) \\ I_3 & = -AJ_e exp(-\phi V_1) + AJ_i(V_3) \\ I_4 & = -A_{i,4}J_e exp(-\phi V_1) + A_{e,4}J_i(V_4) \end{cases} \tag{2.4}$$

where,

$$\phi = \frac{e}{kT_e} \tag{2.5}$$

$$J_e = n_e e\sqrt{\frac{kT_e}{2\pi m_e}} \tag{2.6}$$

The electron temperature appears in each current equation as the ratio of the electron charge to its temperature, as expressed in Equation. 2.5. The electron saturation current density, J_e, defined by Chen [6] in Equation 2.6, is due to thermal diffusion of electrons to each probe. The ion saturation current density, J_i, was assumed to be constant if the most positive probe potential, P_1, satisfies the inequality in Equation 2.7. V_0 was used by Chen [6] as the condition for ion sheath formation. This is also known as the Bohm Sheath Criterion. The geometric surface area or current collection area for each probe is A, k is the Boltzmann

constant, e is the electron charge, and m_e is the mass of an electron.

$$V_l < V_p - V_0 = V_p - \frac{1}{2\phi} \tag{2.7}$$

Note that the collected current by P_4 had different collection areas for ion and electron currents. Burton applied a correction factor of $1/\pi$ to the probe's surface area for the ion current collection area and used $1/2$ for the electron current collection area. For supersonic flow the collection area is reduced due to a wake region of low ion and electron density behind the probe. Ions cannot penetrate this region for a Mach numbers greater than 3 [5]. For the QLP analysis in this paper, Burton's equations are used to determine the electron temperature, density, and ion speed.

Electron Temperature

Burton follows Chen's analysis using the currents from Equation 2.4. Burton assumes that the geometric surface area for each probe is equal and the ion saturation current density is constant regardless of the probe potential [5]. The voltage applied to P_3 and P_4 are the same. Following these assumptions, Equation 2.8 is derived as an implicit equation that can be solved to find the instantaneous electron temperature of a plasma.

$$1 = \frac{1 + exp(\phi V_{d3}) - 2exp(\phi(V_{d3} - V_{d2}))}{\frac{1}{\pi}exp(\phi(V_{d3} - V_{d2})) - \frac{1}{2}} \tag{2.8}$$

Equation 2.8 was derived by taking the ratio of the difference of the current collected by P_1 and P_3, with the current from P_4. This ratio should be one by Kirchhoff's current law. The electron temperature can be calculated because at any instant, equation 2.8 is true. Thus, despite V_{d3} and V_{d2} being time dependent variables, measuring each voltage at a given moment provides the electron temperature at that time.

Electron Density

The electron density is determined indirectly by considering a mechanism from ion sheath formation [6]. If the probe voltage remains V_0 below the plasma potential then entire sheath has been formed. Thus the ion current density can be written as Equation 2.9 for a Maxwellian electron energy distribution [5]. This is a result of the Bohm Sheath Criterion for plasmas when $T_e >> T_i$.

$$j_i = en_e\sqrt{kT_e/m_i}exp(-\frac{1}{2}) \tag{2.9}$$

This current is larger than what can solely be from ion thermal diffusion. Burton asserts that writing expressions for j_e and j_i and solving for each probe gives Equation 2.10 for electron density [5].

$$n_e = \frac{3I_3\sqrt{m_i}exp(\frac{1}{2})}{2Ae\sqrt{kT_e}[exp(\phi V_{d2}) - \frac{\pi}{4}]} \tag{2.10}$$

The measured values of I_3 and V_{d2} can be used to find the instantaneous electron density, n_e. Both Equation 2.9 and by extension Equation 2.10 assume that the ion temperature is negligible compared to the electron temperature.

Ion Velocity

Johnson and Murphree [15], test a version of Kanal's [17] equation for the current collection perpendicular probes in flowing plasmas. They proved that the ion speed can be determined by taking the ratio of the ion saturation current collected by a perpendicular probe with that of a parallel probe. Burton uses Johnson and Murphree's equation for the ion speed, seen in Equation 2.11.

$$\frac{I_\perp}{I_\parallel} = \frac{2A_\perp}{\sqrt{\pi}A_\parallel} exp(-M_i^2) \sum_{n=0}^{\infty} (\frac{M_i^n}{n!})^2 \Gamma(n + \frac{3}{2}) \tag{2.11}$$

Where, $M_i = u_i/c_m$ is the Mach number, and Equation 2.12 is the most probable thermal ion sound speed [9].

$$c_m = \sqrt{\frac{kT_e}{m_i}} \tag{2.12}$$

Equation 2.11 assumes Maxwellian electron and ion distributions. Equation 2.11 requires that the ratio of currents is greater than one, $\frac{I_\perp}{I_\parallel} > 1$, and that the Mach number is greater than three, $M_i > 3$ [5]. It is important to note that Burton models the collected ion saturation current using two different methods when calculating the electron temperature and ion

Mach number.

Plasma Potential

The plasma potential was not measured directly. Instead it was calculated based on Equation 2.13 from plume measurements. Specifically, the electron temperature and floating potential. In a paper by Beal, this model of the plasma potential has shown good agreement relative to the measured plasma potential from an emmissive probe [2]. However, this equation tends to over predict the plasma potential by about 10% according to Beal's results.

$$V_p = V_f + |\frac{k_b T_e}{e} ln(\sqrt{\frac{2\pi m_e}{m_i}} exp(-\frac{1}{2}))| \tag{2.13}$$

2.2.2 Evaluation of assumptions

Many assumptions were presented in QLP theory that take advantage of ideal conditions during data collection. This section will discuss the assumptions made in QLP theory related to ideal Langmuir probe operation and analysis. These assumptions will be used later to discern the validity of the QLP's measurements in the results.

Maxwellian Energy Distribution

To judge the reasonableness of a Maxwellian electron energy distribution, Burton [5] states that the electron-electron collision mean free path must be evaluated and compared to the ion sheath thickness and probe radius. If, $\lambda_{ee}/r_p >> 1$, then the probe is operating in the collisionless regime for electron-electron collisions. In that case, the probe would be receiving an accurate measurement of the plasma parameters from the unperturbed plasma. Thus,

it would be unlikely for any ionization or recombination events to occur within the probe sheath. This is true for other types of collisions that satisfy the same criterion.

A Maxwellian distribution is a common assumption in plasma theory. By assuming a Maxwellian distribution of a particular species means that it is in local thermal equilibrium. In which case measuring the lower order moments of a distribution function, like density, speed, and pressure, in addition to the electromagnetic fields, is enough to quantify a plasma of that species [13]. However, plasmas consist of more than one species; electron, ions, and neutrals. Therefore making measurements of the lower moment quantities for each species is needed to quantify the multi-fluid plasma. Since ions and electrons are coupled through electromagnetic forces their moments are not independent. For example, the principle of quasi-neutrality is related to each plasma species' density and the principle of Ampere's law relates each species' velocity. However, the pressure and temperature between plasma species is not strongly coupled because other energy transport phenomena can transfer more energy faster than collisions between plasma species. In general, a distribution function is important, Maxwellian or not, because its moments describes average physical quantities of that species.

The electron temperature, electron density, and ion speed can all be measured by a QLP. Thus relying on previously made assumptions, i.e. an electron's mobility being greater than the ion mobility, then the electron plasma is almost fully characterized by one diagnostic. Of course, this assumes that the electrons are Maxwellian, which relies on the electron mean free path criterion presented by Burton [5]. The electron current equations modelling each probe relies on a Maxwellian distribution for the electron density and for the average speed of electrons. The Bohm Sheath Criterion also relies on a Maxwellian electron energy distribution.

Thin-Sheath/Bohm-Sheath Criterion

The thin sheath assumption allows for the use of ideal Langmuir probe theory if the sheath is fully formed as satisfied by the Bohm sheath criterion. Essentially the Bohm sheath criterion states that ions move through the sheath at the Bohm velocity, $v_B = \sqrt{eT_e/m_i}$ [23]. This velocity is a result of solving Poisson's equation for the charge distribution between the probe surface and sheath's edge. This is done by assuming quasi-neutrality in the pre-sheath plasma and energy conservation of initially stationary ions. Bohm determined that only probes biased to $V_0 = 1/2\phi$ below the plasma potential will have a fully developed ion sheath. Thus the ion saturation current will be equivalent to Equation 2.9.

Sheath size is also important in terms of spacing between each probe. To have ideal sheath conditions the sheath of one probe cannot breach the sheath of another. Therefore, Equation 2.14 was used to determine the sheath thickness and moreover the proper spacing between probes such that no sheath interactions occurred [8, 33]. If the probe spacing is within the sheath thickness then interactions between sheaths would be possible, compromising ideal Bohm sheath conditions.

$$d_s = \frac{\sqrt{2}}{3}\lambda_D\left(\frac{2e(V_l - V_p)}{kT_e}\right)^{3/4} \tag{2.14}$$

Where, the Debye length is expressed in equation 2.15,

$$\lambda_D = \sqrt{\frac{\epsilon_0 kT_e}{n_e e^2}} \tag{2.15}$$

The difference between, the probe potential, V_l, and the plasma potential, V_p, was estimated to be about 10-45 V when considering the sheath thickness. The electron temperature and density was estimated to be about 3.9-9.4 eV and 4.7-8.6 $\times 10^{15}$ m^{-3} based on preliminary single Langmuir probe data taken from the plume of an electron cyclotron resonance thruster [29]. This led to a calculated max sheath thickness of about 0.09 cm. When the probe spacing was considered, a factor of 10 was applied to this value to ensure no sheath interactions occurred.

Although the sheath can be a few Debye length's thick, Langmuir probe thin-sheath theory is commonly determined by the ratio of the probe radius to the Debye length. Initially, quadruple Langmuir probe data was analyzed assuming $r_p/\lambda_D \sim 45$ was enough to satisfy the thin-sheath condition [4]. More recently, if the ratio of probe radius to Debye length was greater than 100, $r_p/\lambda_D > 100$, then thin-sheath Langmuir probe theory could be used. Otherwise, a Laframboise fit to the collected current would be more ideal for ratios, $5 < r_p/\lambda_D < 100$ [8, 23, 33]. For this paper, thin-sheath theory was used if the probe radius to Debye Length did not fall below 5.

Collisionless Plasma

A plasma is considered collisionless if the probe radius was much less than mean free path for all types of collisions. Collisions between like charges, unlike charges, and charges with neutrals were considered. If , $r_p << \lambda$, remains true for all collisions, then it would be improbable for collisions to occur within the sheath of the probe. Thus collisional effects can be ignored and ideal collisionless QLP theory can be applied to probe measurements. The mean

free paths between charged species were calculated by taking mean thermal speed of the particle and dividing by the collision frequencies as seen in Equation 2.16 [25]. Zwahlen used this method in conjunction with the collision frequencies in Equation 2.17 given by Jones [33, 16].

$$\begin{cases} \lambda_{ee} & = \frac{c_e}{\nu_{ee}} \\ \lambda_{ei} & = \frac{c_e}{\nu_{ei}} \\ \lambda_{ii} & = \frac{u_i}{\nu_{ii}} \end{cases} \tag{2.16}$$

$$\begin{cases} \nu_{ee} & = \frac{16\sqrt{\pi}}{3} n_e (\frac{4kT_e}{m_e})^{-3/2} (\frac{e^2}{4\pi\epsilon_0 \frac{m_e}{2}})^2 ln(\Lambda) \\ \nu_{ei} & = \frac{16\sqrt{\pi}}{3} n_e (2k(\frac{T_e}{m_e} + \frac{T_i}{m_i}))^{-3/2}) (\frac{e^2}{4\pi\epsilon_0 \frac{m_i m_e}{m_i + m_e}})^2 ln(\Lambda) \\ \nu_{ii} & = \frac{16\sqrt{\pi}}{3} n_e (\frac{4kT_i}{m_i})^{-3/2} (\frac{e^2}{4\pi\epsilon_0 \frac{m_i}{2}})^2 ln(\Lambda) \end{cases} \tag{2.17}$$

The mean thermal speed for each species in Equation 2.18 is derived from taking the first moment of a Maxwellian distribution.

$$c_q = \sqrt{\frac{8kT_q}{\pi m_q}} \tag{2.18}$$

Where q is the species being considered. In Equation 2.17 the coulomb logarithm was assumed to be about 14 based on a common value of the logarithm for electric propulsion type plasmas in Rutherford [11]. The electron to ion temperature ratio was assumed to be 100. However, this assumption did not take into account the minimum propellant temperature entering the Hall thruster. The minimum propellant temperature was assumed to be 300 K

or the temperature of the lab. For an electron temperature of 1 eV, this assumption puts the ion temperature at 116 K. This ion temperature is much less than the initial temperature of the propellant. Equation 2.16 assumes that the electron to ion temperature ratio is greater than or equal to 1 and less than or equal to 100 [33]. The assumed temperature ratio lies within this range and Equation 2.16 can be used to calculate mean free paths between charged species. For the ion-ion collision mean free path the ion velocity was used if it was greater than the mean thermal speed based on the assumed temperature of the ions. This occurred for about 88% of the data points in one measurement trace.

All neutral collision mean free paths were estimated using Equation 2.19. This is a more generalized definition of collisional mean free paths between species [11]. By Equation 2.19, the mean free path is equal to the inverse of the product between the density of the neutrals and the size of their cross-sectional area.

$$\lambda_{nn,en,in} = \frac{1}{\sigma n} \tag{2.19}$$

The radius of Xenon neutrals was taken to be 108 pm. The density was calculated using the ideal gas law. The temperature of Xenon was assumed to be at 25 ^{o}C. Measurements of pressure were taken with a nude ion gauge calibrated for air. Pressure measurements were corrected using a correction factor of 2.87 for Xenon. The measured background pressure of Xenon was dependant on the mass flow rate output from the Hall thruster. Common pressures were 41, 52, and 55 μTorr.

End Effect for Flowing Plasmas

Since there are multiple probes in the system that need to be aligned with the flow, it is important that the probe was designed to ensure alignment. However, ion currents collected by the probes parallel to the flow with a sufficient end effect parameter are not sensitive to a small misalignment [7, 8, 33]. This is the case provided that the end effect parameter, τ_L in Equation 2.20 is larger that 50. The end effect parameter is given by

$$\tau_L = \frac{L_p}{\lambda_D} \frac{\sqrt{\frac{kT_e}{m_i}}}{u_i} >> 50 \tag{2.20}$$

where the ratio of the probe length, L_p, with the Debye length, λ_D, is multiplied by the ratio of the Bohm speed to the ion speed. This condition was used with the preliminary single Langmuir probe measurements to design the probe lengths of the QLP.

Current Collection of Supersonic Plasma

Both ion and electron current collected by the perpendicular probe in a supersonic plasma only depend on a fraction of the geometric surface area. The collection area is reduced by a wake region of different electron and ion densities behind the perpendicular probes [5]. However, a correction factor for the ion and electron current collecting area of a probe is not needed in a flow with a mach number less than 3, $M_i < 3$ [28]. Therefore, by requiring that Equation 2.11 be used when $M_i > 3$, then a correction factor of π and 2 can be implemented for the collected ion and electron current, respectively.

Langmuir Probes in Magnetic Fields

When a Langmuir probe is in a magnetic field the electrons are the first species of a plasma to become magnetized. Thus the collected electron current will be affected. If the local Larmor radius of the electrons is much greater than the probe radius then the collected electron current is unaffected [23]. For making measurements where the magnetic field is not negligible a cylindrical Langmuir probe should be aligned such that its collection surface is normal to the magnetic field. This would reduce the effect magnetic field has on Langmuir probe measurements because the effective probe collection area is a function of the area normal vector with the normalized magnetic field vector. In the case of the QLP presented in this thesis, it was positioned about 6 Hall thruster diameters away from the thruster along its centerline and it was assumed that the magnetic field would negligible. Thus the Larmor radius of any magnetized electron behavior would be guaranteed to be larger than the probe radius. Therefore any effect of the magnetic field on measurements by the QLP were not considered in the analysis.

As stated previously, each of the assumptions provided from QLP theory depend on the parameters being measured. Therefore, the parameters must be estimated to determine the size of the QLP. The electron temperature and density were estimated from single Langmuir probe data from SPACE lab's Electron Cyclotron Resonance thruster [29]. As previously stated the electron temperature and density were calculated to be 3.9-9.4 eV and 4.7-8.6 $\times 10^{15}$ m^{-3}, respectively. The plasma potential and the floating potential were estimated to be between 34-45 V and 14-26 V, respectively. The ion speed was estimated to be around 10 km/s. These plasma parameters were used to design the QLP.

2.3 QLP Design

The SPACE lab Quadruple Langmuir Probe (QLP) used cylindrical 0.234 cm diameter graphite probe tips. These probe tips have a length of 4.5 ± 0.2 cm. The collection area or surface area of each probe was 3.3 ± 0.2 cm^2. Spacing between the probes was chosen to be 0.93 ± 0.1 cm, which was 10 times the estimated sheath thickness. The entire length of the probe was 19.5 cm from the probe stand to the probe tips to reduce the effect of the stand on the plasma parameters. BNC cables attached to the back of the probe and transported signal through vacuum feed-through ports to the QLP circuit, represented by Figure 2.3.

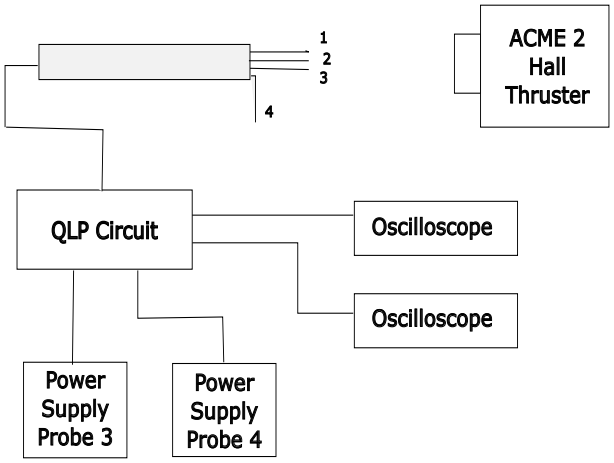

Figure 2.3: Generalized Experimental setup of the probe system.

Two DC power supplies capable of supplying up to 30 volts were used to bias both P_3 and P_4 independently. Both probes were negatively biased relative to P_1. Measurements were taken on two separate oscilloscopes which measured V_1, V_{d2}, V_{d3}, V_{d4}, I_3, and I_4.

Both scopes measured V_{d2} in an attempt to synchronize each scope. This method of synchronization resulted in only two of sixteen trials being synchronized, one of which will

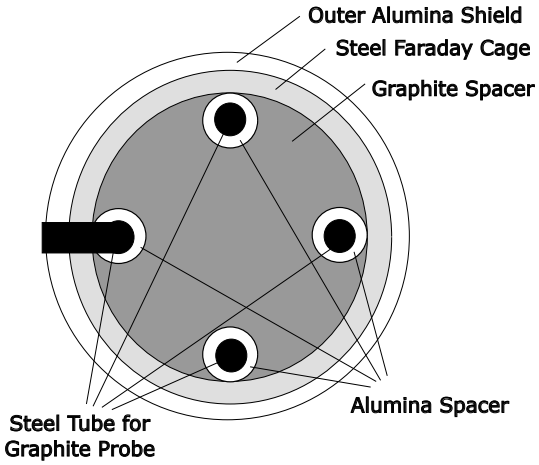

Figure 2.4: A not to scale frontal view of the QLP without the graphite probes tips or the Boron-Nitride spray on coating.

be presented in the results section. A disruption of the measured signal in V_{d2} seemed to cause the synchronization. If only steady state Hall thruster operation is being measured, synchronization should be achieved by using a pulse generator to trigger both scopes. However, this was not done in this thesis.

This QLP was designed to use graphite probe tips to measure highly reactive plasmas containing atomic oxygen. Other QLPs used tungsten probes, which need to be cleaned between testing to reduce the amount of oxidized tungsten on probe surfaces [5]. Graphite was used because oxidized carbon does not stick to the probe and thus the probe does not lose conductivity due to oxidation. This design allows Graphite probes to be replaced once sufficient erosion is evident. The probe tips are held in place by steel tubes using a friction fit. Figure 2.4 is a front view of the QLP without the graphite probe tips and the Boron-Nitride spray-on coating.

Alumina tubes hold the steel tubes to electrically isolate the signals from each other. A

graphite spacer holds the alumina tubes to the inner side of a steel tube which acts as a Faraday cage. The Faraday cage protects the signals of all four probes from plasma induced noise. An alumina tube telescopes over the steel Faraday cage to protect it from the hot plasma. A Boron Nitride Coating was sprayed onto the graphite spacer, but not over the steel tubing.

2.3.1 QLP Circuit

The circuit for the QLP seen in Figure 2.5 was designed to bias P_3 and P_4 to the same potential relative to P_1. This circuit incorporates shunt resistors to measure the currents collected by P_3 and P_4. Capacitors were installed in parallel with the power supplies to limit the effect of plasma induced noise in the supplied DC signal and to source additional current for the experiment [18]. The resistors to ground were not needed, but also do not affect the current measurements across the shunt resistors. This was because the current collected from the probes was on the order of milli-amps whereas the current through the resistors to ground was on the order of micro-amps.

From QLP theory, the biases from P_1 could not exceed the plasma potential. P_2 was not biased and free to stabilize at the floating potential during testing. Whereas, P_3 and P_4 remained below the floating potential. To apply the appropriate biases to P_3 and P_4 both power supplies were set to 26.89 V as measured by a handheld digital multi-meter. The shunt resistors had resistances of 1 kΩ and resistors to ground had resistances of 1 MΩ.

2.4 Operating Procedures

A brief summary of the steps used to acquire the measured data and a discussion of the synchronization method used between two oscilloscopes is provided. Additionally, an ac-

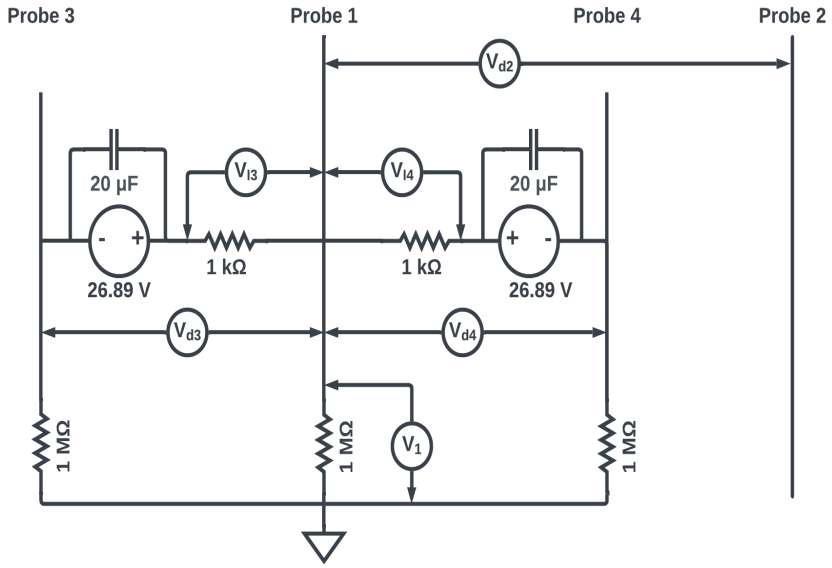

Figure 2.5: The QLP circuit schematic. The same negative potential was applied to probes 3 and 4 to collect ion saturation current. Probe 2 was unbiased and was allowed to acquire the plasma floating potential. Probe 1 had a positive potential relative to the floating potential.

count of the equipment used and their settings are provided below. This section discusses the procedures used during testing.

Measurements where taken with two floating TPS-2024B oscilloscopes. Seven channels between two oscilloscopes used TPP0201 10x probes to measure voltage signal from the QLP. Measurement locations are depicted in Figure 2.5. The oscilloscope probes made each measurement with their reference lead attached to probe 1 of the QLP. Except for one oscilloscope probe which measured the potential of probe 1 relative to ground. The circuit was powered by two independent DC power supplies. DC power supply model HJS-480-0-48 was capable of the providing up to 48 V and Electro-Industries' regulated DC power supply model 3002A was capable of providing up to 30 V. Again the voltage difference between the

electrostatic probes 3 and 4 of the QLP had to be the same. Therefore, the supplied voltage was set to be equivalent as measured by a OW18B handheld Digital Multi-Meter. The measured voltage supplied by each power supply was 26.89 V. Each oscilloscope was set to acquire one sample of each signal. Each scope would be triggered by the floating voltage signal.

Both oscilloscopes measured the voltage difference between the electrostatic probe 1 and 2 on the QLP. This was done in an attempt to use that signal to synchronize each oscilloscope because the floating potential was thought to be dependent in time due to a Hall thruster breathing mode. However, only two of sixteen total trials were synchronized with this method. It was determined that a pulse generator should be used to synchronize the oscilloscopes on their external trigger for steady state operation of the Hall thruster. The time scale of each oscilloscope was set to collect about five cycles of the maximum expected breathing mode around 30 kHz. Scope traces were collected for each of the Hall thruster operating conditions.

Chapter 3
RESULTS

One of the primary objectives of this campaign was to capture the breathing mode. All measurements were conducted for the same QLP operating conditions and for a Hall thruster operating in a steady-state condition. Probes 3 and 4 were biased to 26.89 V. The QLP was positioned along the centerline, at a distance of 6 thruster diameters from the exit plane of the Hall thruster. The frequency range of the breathing mode in a Hall thruster was assumed to be between 10 and 30 kHz. The scopes were set to measure a total time interval of 250 μs to capture a few cycles of the breathing mode. This section provides a discussion of the data reduction, the results, and the uncertainty analysis.

3.1 Data Processing and Reduction

Data from the oscilloscopes existed in .csv format for each channel across oscilloscopes. Each file was read by a Matlab algorithm which organized each measurement into a matrix whose columns represented a particular trial. Certain data sets were excluded due to poor synchronization efforts. Measurements from trials 1, 2, and 4-15 were not properly synchronized across oscilloscopes. Trials 3 and 16 were synchronized due to a disruption in the plume of the Hall thruster. All operating parameters of the Hall thruster can be seen in Table 3.1. A moving average was applied to each trial to reduce the noise in their measurements. The window for the moving average was chosen to be 7 integers, or 0.28% of the data points per trial. This reduced most of the noise and allowed for better calculations of the instantaneous electron temperature, density, and ion speed. With the noise reduced, the Hall thruster

breathing mode was more prevalent, as seen in the next section.

Moreover, positive ion saturation current was neglected from the analysis. Since, ion saturation current must be negative then any positive current collected by the negatively biased probes must be neglected. This measured positive ion saturation current, may have caused the synchronization of the two oscilloscopes. Finally, the current ratios greater than the numerical solutions of the summation in Equation 2.11 were removed from the analysis.

3.2 Data Analysis

Although only trials 3 and 16 were synchronized, only data from trial 3 will be discussed here. This is because trial 3 was a part of the normal Hall thruster operating regime whereas trial 16 was a small part of a cathode flow test whose flow rate was far greater than normal operating conditions. The Hall thruster operating parameters for trial 3 and 16 are provided in table 3.1. The evaluation for the electron temperature and density closely follows Burton's analysis [5]. The calculation of the plasma potential were based on Equation 2.13, which models the plasma potential based on the electron temperature and floating potential [2]. A brief summary of the current and voltage data is provided in Table 3.2.

The filtered instantaneous current and voltage data was used to solve Burton's equations for the electron temperature and density, using Equation 2.8 and Equation 2.10, respectively [5]. Those measurements were also used to determine the ion speed by solving Equation 2.11 which was originally presented by Johnson and Murphree [15]. The electron temperature

Trial	Discharge Voltage	Anode Flow Rate (sccm)	Cathode Flow Rate (sccm)
1	250	14	3
2	250	16	3
3	250	18	3
4	300	14	3
5	300	16	3
6	300	18	3
7	350	14	3
8	350	16	3
9	350	18	3
10	400	14	3
11	400	16	3
12	400	18	3
13	300	16	5
14	300	16	8
15	300	16	13
16	300	16	15

Table 3.1: All operating parameters of the Hall thruster.

	V_1 (V)	V_{d2} (V)	I_3 (mA)	I_4 (mA)
Min	2.4	-2.9	-3.1	-7.1
Max	5.8	-0.85	1.7	-1.0
Mean	4.4	-1.9	-1.1	-4.3

Table 3.2: Summary of current and voltage data measured by the QLP.

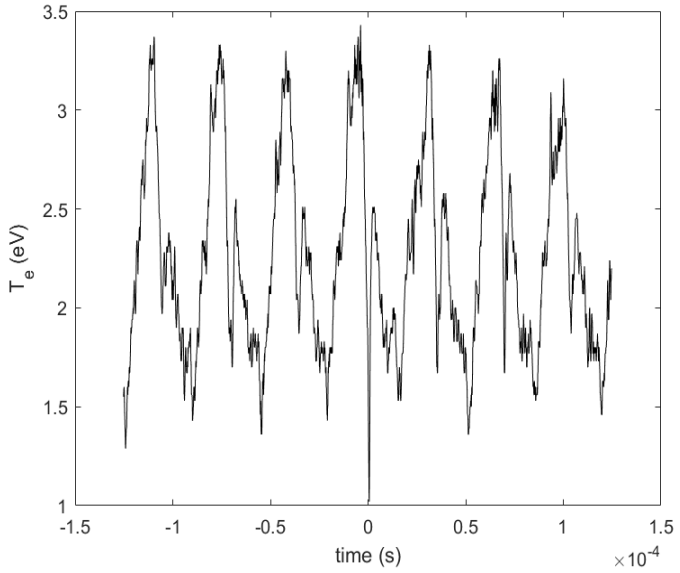

Figure 3.1: Instantaneous electron temperature for the ACME Hall thruster operating at steady state for a discharge voltage of 250 V, an anode flow rate of 18 sccm, and a cathode flow rate of 3 sccm.

and ion speed were numerically solved as non-linear implicit equations. Once the electron temperature was known the plasma potential was solved using Equation 2.13.

The instantaneous electron temperature for the ACME Hall thruster operating in steady state is given in Figure 3.1. Operating conditions for the Hall thruster consisted of a discharge voltage of 250 V, a discharge current of 1.403 A, an anode flow rate of 18 sccm, and a cathode flow rate of 3 sccm. Notice the electron temperature changes in a cyclic fashion similar to a breathing mode. An estimation of the frequency of the electron temperature is about 28.4 kHz. This frequency fell within the range of assumed Hall thruster breathing modes.

The breathing mode of a Hall thruster is an ionization instability. As ionization of neu-

trals occurs in the channel due to collisions with electrons, the neutral density decreases and the plasma density and ionization rate increases [20]. If the ionization rate exceeds the rate of neutrals being supplied to the channel, then the neutral density and ionization rate will decrease. The plasma that exists in the channel will be accelerated into the plume region and the plasma density will decrease in the channel. The channel then starts refilling with neutrals from the anode and the ionization rate increases again. A cycle essentially continuing in perpetuity.

The electron temperature varies between 1 eV and 3.4 eV. In a Hall thruster cluster experiment which consisted of four BHT-200-X3 200 W Hall thrusters, the electron temperature was measured at 3.4 eV when the triple probe was positioned 5 cm in front of on of the thrusters [3]. ACME was operating at a power of 350 W when the measurement in Figure 2.8 was taken. From other plume mapping measurements with the same thruster configuration, the electron temperature was measured at 2.5 eV for a QLP position at 32 cm downstream of the cluster [1].

Figure 3.2 was a measurement of the instantaneous density for steady state operation of the ACME Hall thruster. This result was based on Burton's equation for density, Equation 2.10 [5]. This plot depends on the same operating conditions previously mentioned. The measured electron density was on the order of 10^{17} m^{-3} which larger than expected from the single Langmuir probe data taken in an ECR thruster plume [29]. However, it is not uncommon for QLP theory to have larger errors in their density measurement [6]. The breathing mode is still evident in Figure 3.2 and will be for all the time-dependent plots.

Figure 3.3 was the result of solving Equation 2.11 and making an assumption about the most probable thermal ion speed. The ion speed is centered around 20 km/s which is

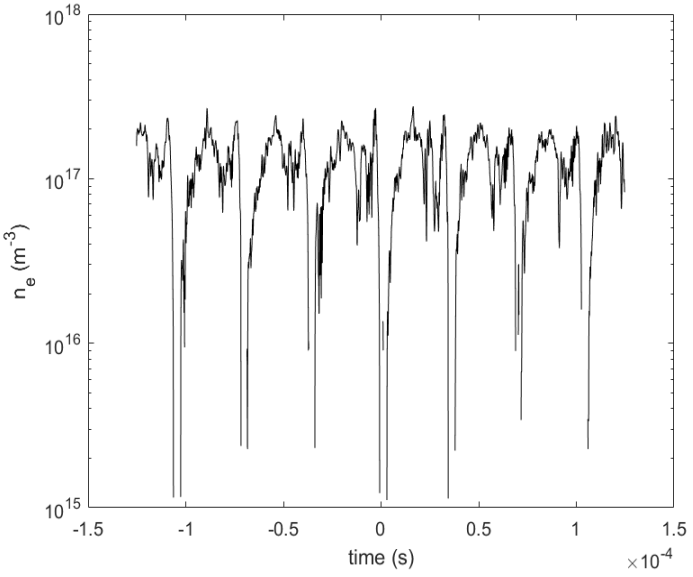

Figure 3.2: Instantaneous electron density for the ACME Hall thruster operating at steady state for a discharge voltage of 250 V, an anode flow rate of 18 sccm, and a cathode flow rate of 3 sccm.

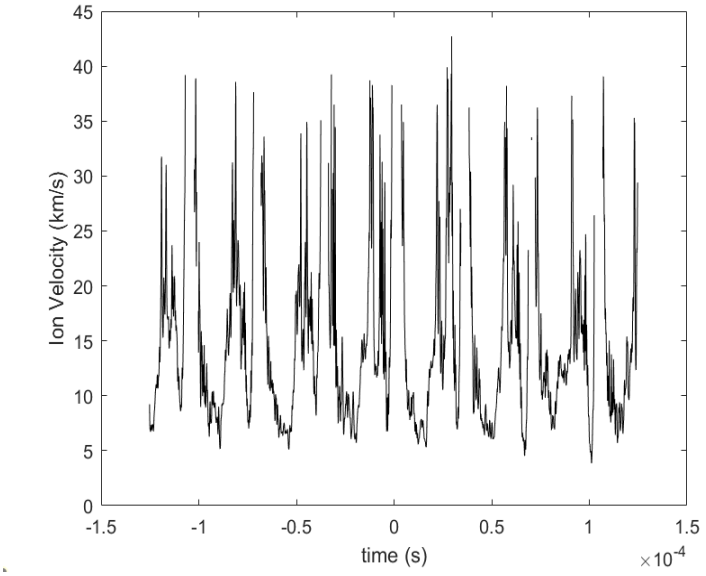

Figure 3.3: Instantaneous ion velocity for the ACME Hall thruster operating at steady state for a discharge voltage of 250 V, an anode flow rate of 18 sccm, and a cathode flow rate of 3 sccm.

expected for a discharge voltage of about 250 V. This most probable thermal ion speed is based on an ion temperature and electron temperature, but since it is assumed that the ion temperature was less than the electron temperature by a factor of 100, the ion temperature was negligible in the determination of the ion sound speed. In some cases this assumes the ion temperature is less than standard lab temperature at 300 K. Thus, in those cases the electron to ion temperature ratio of 100 is a poor assumption. In addition, the ion temperature will be greater than the room temperature due to its ionization from hot electrons in the channel, which will have more of an effect on calculating the most probable ion sound speed.

Note that the ion speed is not directly solved using Equation 2.11 because an assumption is made about the most probable thermal ion speed [5]. Instead, the Mach number is directly

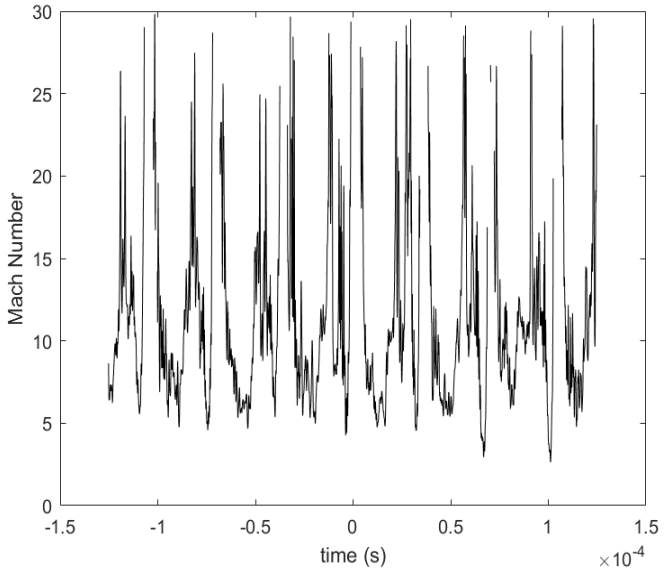

Figure 3.4: Instantaneous Mach number for the ACME Hall thruster operating at steady state for a discharge voltage of 250 V, an anode flow rate of 18 sccm, and a cathode flow rate of 3 sccm.

solved from the measured ion saturated currents collected from P_3 and P_4. Figure 3.4 is the result from solving Equation 2.11. The mean Mach number is 10.9 for operating parameters of trial 3. As seen in Figure 3.4, the Mach number varies between 2.6 and 29.8. Since half of the data is below the mean and within a difference of 8.3, a Mach number above about 20 may not have been a the result of an accurate measurement. Gatsonis and Zwahlen measure a maximum Mach number of 6 using a QLP [8, 33]. Therefore, measuring a Mach number of 20 or greater was not accurate and was due to a sign change in the collected current of probe 3.

For Mach numbers greater than 12 the summation and the exponential term in Equation 2.11 were approximated based on numerical trends. This was because for large Mach numbers, the summation needed to compute more than 172 terms. This is the upper limit of the gamma function in Matlab. Thus, calculating Equation 2.11 exactly could only be done up

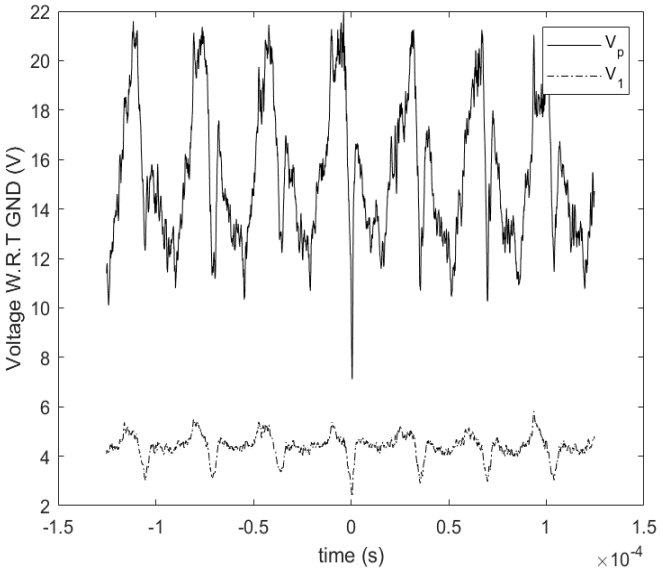

Figure 3.5: Instantaneous plasma potential approximation and voltage applied to probe 1 with respect to ground. ACME Hall thruster was operating at steady state for a discharge voltage of 250 V, an anode flow rate of 18 sccm, and a cathode flow rate of 3 sccm.

to a Mach number of 12. The behavior of this equation was linear with the Mach number so a linear fit was applied to the summation and exponential term. Thus, expanding the capability of Equation 2.11.

Figure 3.5 is an approximation of the plasma potential based on instantaneous values of electron temperature and density. This approximation is based on Equation 2.13 [2]. This equation was used to approximate the plasma potential in the plumes of low powered Hall thrusters.

As seen in Figure 3.5, the plasma potential calculated with respect to ground was larger than the voltage applied to probe 1. Therefore, the applied voltage to probe 1 was not

greater than the plasma potential and standard operation of the QLP had been successfully executed. The fully formed sheath criterion, V_0, stated previously is on the order of the plasma potential with the largest difference at 1.7 V for an electron temperature of 3.4 eV.

For the time-averaged data in Figure 3.6, 3.7, and 3.8, the error bars are the average uncertainty for the synchronized measurements plus one standard deviation and an additional uncertainty for a thick sheath. The evaluation of the assumptions and the uncertainty analysis will be discussed in the next section. Each of these figures have an anode flow rate of 16 sccm and a cathode flow rate of 3 sccm, while the discharge voltage was varied. These operating parameters are shown in Table 3.1.

Figure 3.6 is the time-averaged electron temperature over different operating conditions. Note that the electron temperature has slight growth with one outlier. The average is 2.6 $\pm$ 0.1 eV for a discharge voltage range of 250 V to 400 V. This consistent electron temperature could be due to the cathode production of electrons. The cathode flow rate was held constant for each discharge voltage. Thus, the electron temperature for the electrons that escape from the cathode into the plume may only be dependent on the operating conditions of the cathode.

Figure 3.7 shows the time-averaged electron density. As the discharge voltage increases the electron density in the plume decreases. Increasing the discharge voltage of the anode could mean that more electrons are pulled into the Hall channel and ionizing propellant. Thus, causing a decrease in electron density in the plume.

Figure 3.8 shows the time-averaged ion velocity. Figure 3.8 also has a theoretical calculation for the xenon ion velocity from electrostatic acceleration by that discharge voltage. For

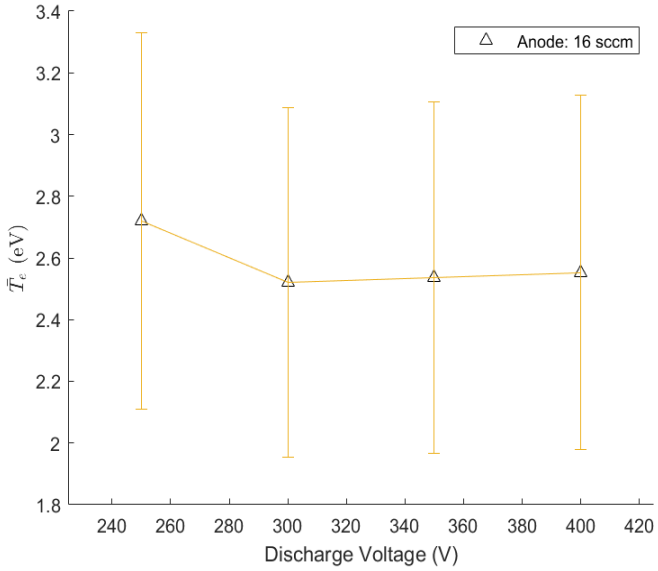

Figure 3.6: A time-averaged plot with a standard deviation of the electron temperature at different Hall thruster discharge voltages and an anode flow rate of 16 sccm.

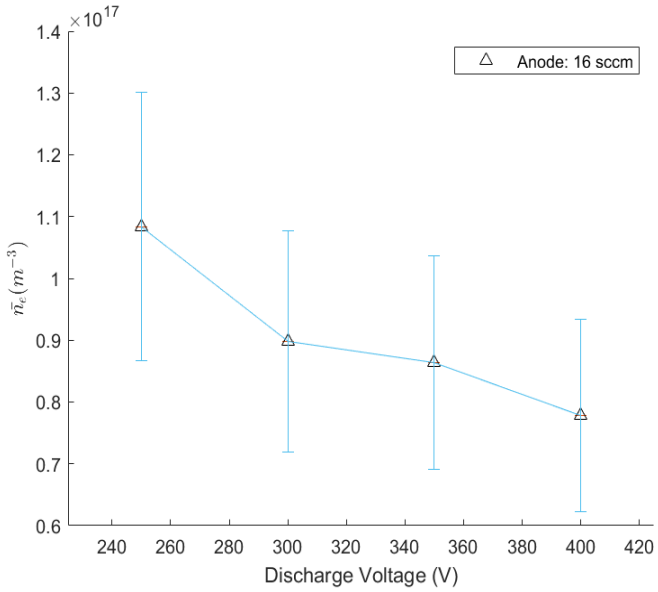

Figure 3.7: A time-averaged plot with a standard deviation of the electron density at different Hall thruster discharge voltages and an anode flow rate of 16 sccm.

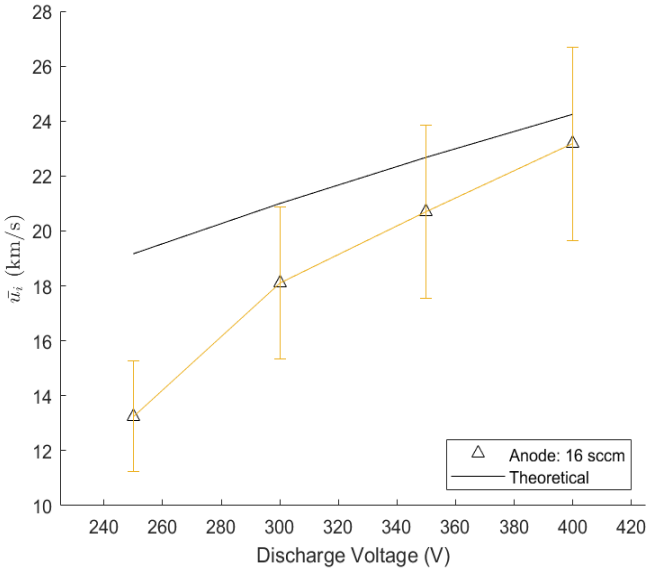

Figure 3.8: A time-averaged plot with a standard deviation and fit for the ion velocity at different Hall thruster discharge voltages and an anode flow rate of 16 sccm.

higher discharge voltages the measured and theoretical result have better agreement, but the measured result under predicts the ion velocity for each operating voltage. This measured ion velocity could stem from the ions having been accelerated from an anode floating voltage that was lower than the discharge voltage out to the plasma potential. In which case the ions would have been accelerated by a smaller potential difference than the operating discharge voltage. In addition, if the propellant is not ionized at the anode then the neutral particles will have already traversed a portion of the electric field in the channel before being ionized. The average error between the theoretical and the measure velocity was about 14%.

3.3 Uncertainty Analysis

Each of the results presented thus far have come from ideal thin-sheath quadruple Langmuir probe theory. There are many important plasma scale-lengths that need to be considered before the base analytical uncertainty can be calculated. Scale-lengths such as the Debye length, mean free paths of collisions, and the sheath thickness. If all of the assumptions are satisfied then the analytical uncertainty can be taken into account. An uncertainty analysis by Gatsonis was applied to Burton's and Beal's equations for the measured plasma parameters. In short, for each equation the derivative is taken with respect to each measured parameter. Then the sum of the products of the derivative and its corresponding measurement uncertainty is taken [8, 33]. The uncertainty of the plasma parameter can then solved. In this section each assumption made in the QLP theory will be evaluated and the results of the uncertainty analysis will be discussed.

To consider how well the thin-sheath Langmuir probe theory applied to the results, the probe radius to Debye length ratio was evaluated. The Debye length was calculated by Equation 2.15 and the probe radius was 0.117 cm. Ideal thin-sheath Langmuir probe theory is used in practice for $r_p/\lambda_D > 100$ [33]. This was due to Laframboise's paper on the collected current fits for the transitional regime for these ratios, $5 < r_p/\lambda_D < 100$ [21]. Other initial QLP papers use the condition of $r_p/\lambda_D > 1$, for utilizing conventional Langmuir probe theory [4]. Figure 3.9 was the results of the instantaneous probe radius to Debye length ratio.

As seen in Figure 3.9, the average probe radius to Debye length ratio was 33.9 with a maximum of 66. This signifies that the analysis should be redone with transitional Langmuir probe theory. Note this ratio jumps to zero because of the negative results for electron density which stems from the 60 Hz noise from the power supply to probe 3.

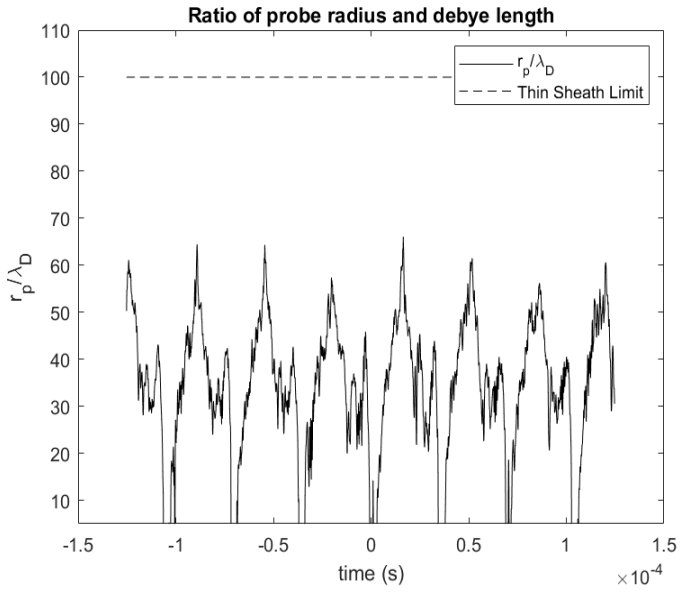

Figure 3.9: The instantaneous probe radius to Debye length ratio, r_p/λ_D to compare with the thin-sheath criterion from literature. Transitional Langmuir probe theory may be more appropriate for these ratios

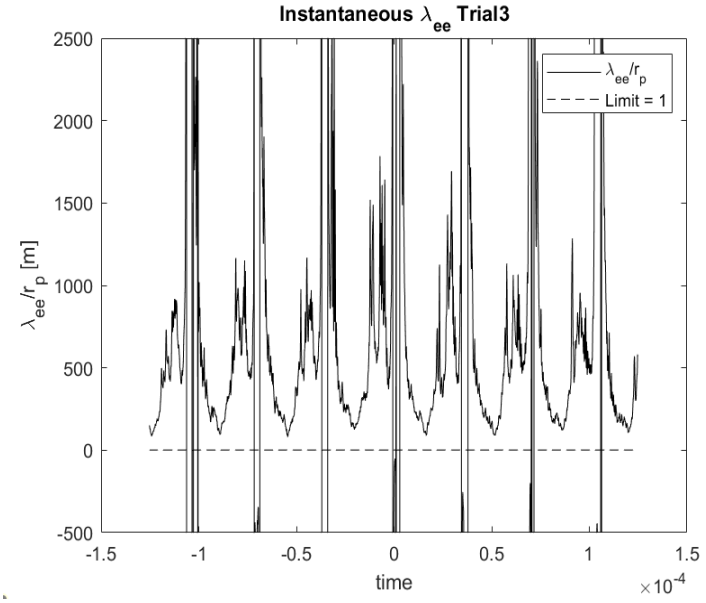

Figure 3.10: The instantaneous normalized electron-electron collisional mean free path, λ_{ee}/r_p.

To confirm that no collisions reside within the sheath of the probes, the collisional mean free paths for different collisions were compared with the probe radius. The mean free path for collisions between charged particles was calculated using Equations 2.16 and 2.17. The sheath is considered collisionless if $\lambda_{mfp}/r_p >> 1$ [5, 4, 8, 33]. Figures 3.10, 3.11, and 3.12 were the results of the instantaneous normalized mean free path for electron-electron, electron-ion, and ion-ion collisions, respectively. Each mean free path was normalized by the probe radius.

For the normalized electron-electron mean free path data, 87% remained mostly between 94 and 2000. Thus, the assumption of Maxwellian electrons is valid. The large jumps in λ_{ee}/r_p were related to the disruption that triggered the oscilloscopes and can be attributed to the presence of noise or the limitations of Equations 2.16 and 2.17. These equations can

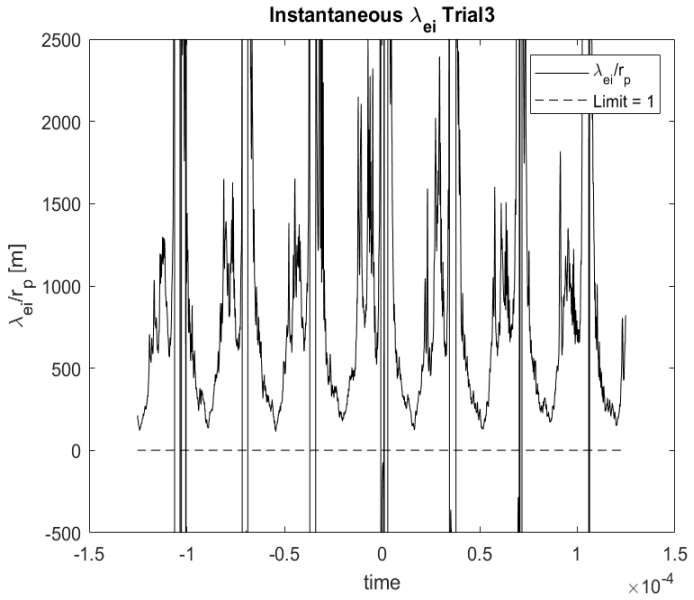

Figure 3.11: The instantaneous normalized electron-ion collisional mean free path, λ_{ei}/r_p.

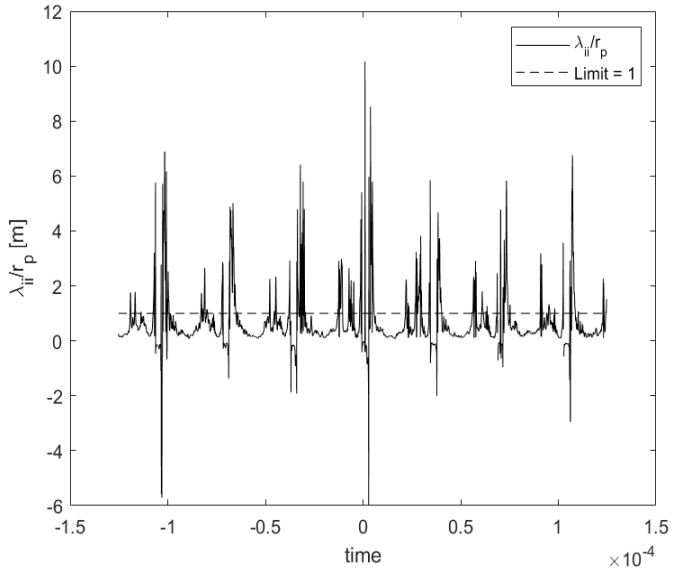

Figure 3.12: The instantaneous normalized ion-ion collisional mean free path, λ_{ii}/r_p.

be considered accurate if $1 \leq T_e/T_i \leq 100$, which was not always the case if a ratio of $T_e/T_i = 100$ and a minimum ion temperature equal to 300 K was assumed. For the normalized electron-ion mean free path data, 83% remained mostly between 120 and 1750. Again the large jumps in this normalized scale length was due to a large amount of noise due to this disruption.

Using Equations 2.16 and 2.17 for the ion-ion mean free path resulted in 85% of the data being below the ideal limit of the collisionless criterion in Figure 3.12. However, in a Hall thruster plume the ion-ion mean free path should be larger than the probe radius and on the order of the election-ion mean free path. Thus, the ion-ion mean free path was re-examined using the approximation in Equation 3.1, which contains an alteration of the approximation from Rutherford [11]. This assumes that $T_e \sim T_i$, which was also within the limits of Equations 2.16 and 2.17. The results of this approximation can be seen in Figure 3.13, where 88% of the data resides within a ratio of 50 and 4000. The calculated ratio of mean free path between neutrals and charged species with the probe radius was found to be 12,900. This result was simply based on background pressure measurements of an ion gauge corrected for Xenon in combination with the ideal gas law and the standard lab temperature at 300 K. Considering all neutrals and pressure measurements of the ion gauge, the mean free path was calculated to be 4500.

$$\frac{\lambda_{ii}}{r_p} \sim \sqrt{\frac{m_i}{m_e}} \frac{u_i \lambda_{ei}}{c_e r_p} \tag{3.1}$$

The end effect parameter will determine how sensitive the parallel probe tips are from a small misalignment to the flow vector of the plasma. If the end effect parameter, τ_L, is greater

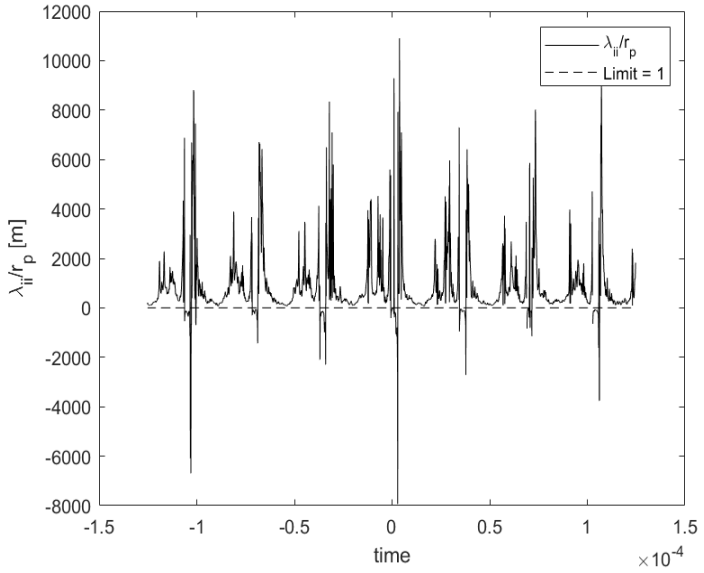

Figure 3.13: The instantaneous approximated normalized ion-ion collisional mean free path, λ_{ii}/r_p.

than 50, then measurements by the probes will not be sensitive to any misalignments during data collection [4, 33]. Zwahlen recorded an end effect parameter range of 200 - 2000, for a probe length of 6 mm. Figure 3.14 was the results of the instantaneous end effect parameter.

In Figure 3.14, 87% of the data remains above the limit of 50. Similar to Zwhalen, depending on the plasma parameters, τ_L varies drastically. The average end effect parameter was 9.6 $\times 10^6$. This was quite large in comparison with Zwahlen. However, the ratio of probe length to probe radius for this QLP was 38.4, which is smaller than other electrode aspect ratios. The aspect ratio of the probe tips for Zwahlen and Gatsonis were about 100, and for Burton the aspect ratio was about 40. Therefore, reducing the length of the probe tips would increase this discrepancy of electrode aspect ratios. For an end effect parameter of this magnitude, it guarantees that a small misalignment of probes and the plasma flow

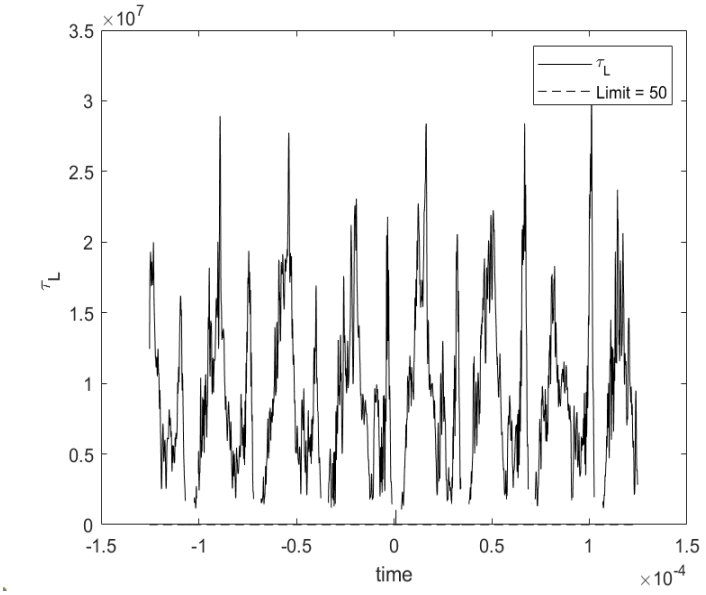

Figure 3.14: End effect parameter, τ_L, for the instantaneous data and criterion from literature.

vector will not significantly affect the collected current.

Finally, the last assumption to evaluate is the sheath thickness and probe spacing. The spacing between the probes was 0.93 cm and was, on average, larger than 39 times the sheath thickness. Zwahlen expected a range of probe spacing to sheath thicknesses ratios of 45 to 14,000. Instead, Figure 3.15 shows the sheath thickness normalized by the probe radius.

In Figure 3.15, for 88% of the duration of trial 3, the sheath thickness remained in the range of 10% to 40% of the probe radius. This adds significant current collecting area to the probe which had not been considered. Due to this sheath thickness error, the electron temperature and electron density can be over predicted by 5% and 15%, respectively [5]. This breakdown of ideal conditions will affect the uncertainty of the measurements in this

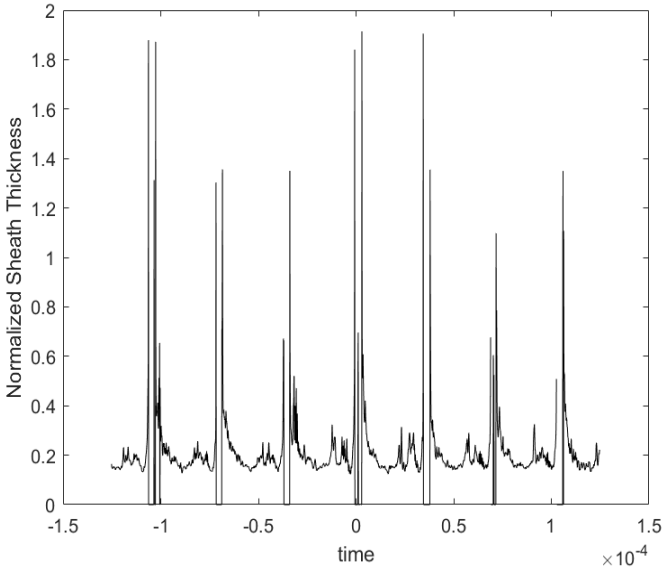

Figure 3.15: The instantaneous sheath thickness normalized by the probe radius.

thesis.

The analytical uncertainty was calculated based on an analysis of implicit non-linear equations conducted by Gatsonis and Zwahlen [8, 33]. Equation 3.2 was solved for the uncertainty of the plasma parameters based on Equations 2.8, 2.10, 2.11, and 2.13 from Burton and Beal.

$$\begin{cases} \frac{\partial f_1}{\partial T_e}\Delta T_e &= -(\frac{\partial f_1}{\partial V_{d2}}\Delta V_{d2} + \frac{\partial f_1}{\partial V_{d3}}\Delta V_{d3} + \frac{\partial f_1}{\partial V_{d4}}\Delta V_{d4}) \\ \Delta n_e &= \frac{\partial f_2}{\partial T_e}\Delta T_e + \frac{\partial f_2}{\partial L_p}\Delta L_p + \frac{\partial f_2}{\partial r_p}\Delta r_p + \frac{\partial f_2}{\partial V_{d2}}\Delta V_{d2} \\ \frac{\partial f_3}{\partial S_i}\Delta S_i &= \Delta(\frac{I_\perp}{I_\parallel}) \\ \Delta V_p &= \frac{\partial f_4}{\partial T_e}\Delta T_e + \Delta V_{d2} + \Delta V_1 \end{cases} \tag{3.2}$$

Where f_1 corresponds to Equation 2.8, f_2 is Equation 2.10, f_3 is Equation 2.11, and f_4 is

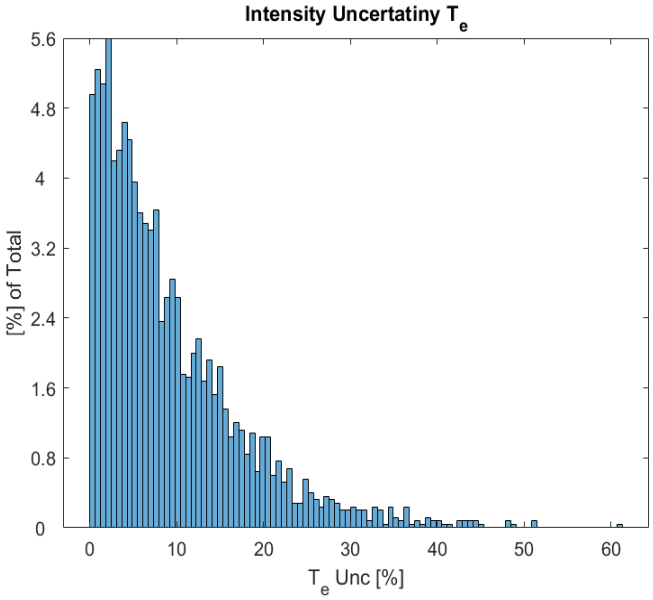

Figure 3.16: Histogram of the uncertainty of the electron temperature as a percentage of the total number of data points.

Equation 2.13. The uncertainty for the ion velocity was calculated in a similar fashion since it is equivalent to the product of the Mach number and the most probable ion speed. The results of the analytical uncertainty are presented in figures 3.16, 3.17, 3.18, 3.19, and 3.20. The measurement uncertainty terms also account for the moving standard deviation during signal filtration of the voltage and current signals.

The average analytical uncertainty for the electron temperature was ±9%. This is greater than the uncertainty of the electron temperature predicted by a sheath that is in the transitional regime, which was ±5% [5]. Based on these uncertainties, the total uncertainty for the electron temperature should be ±14%. This was determined by summing the analytical uncertainty and the uncertainty associated with a large sheath. The uncertainty of Burton's electron temperature measurement was ±23% which relates multiple sources of error. The

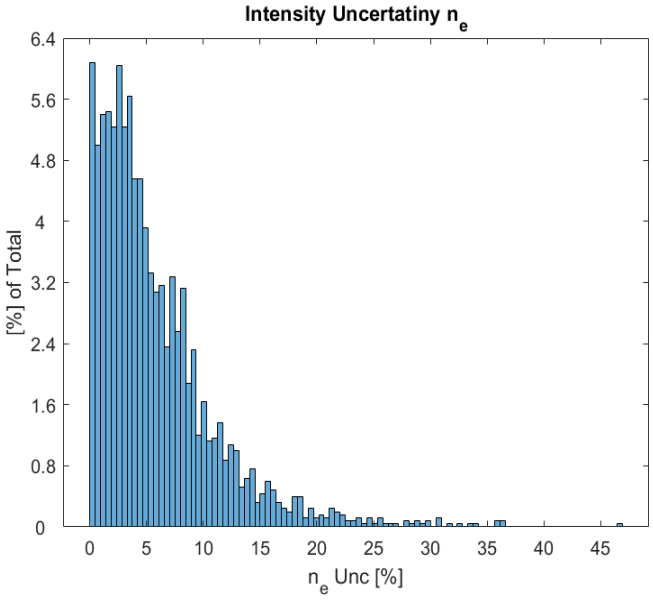

Figure 3.17: Histogram of the uncertainty of the electron density as a percentage of the total number of data points.

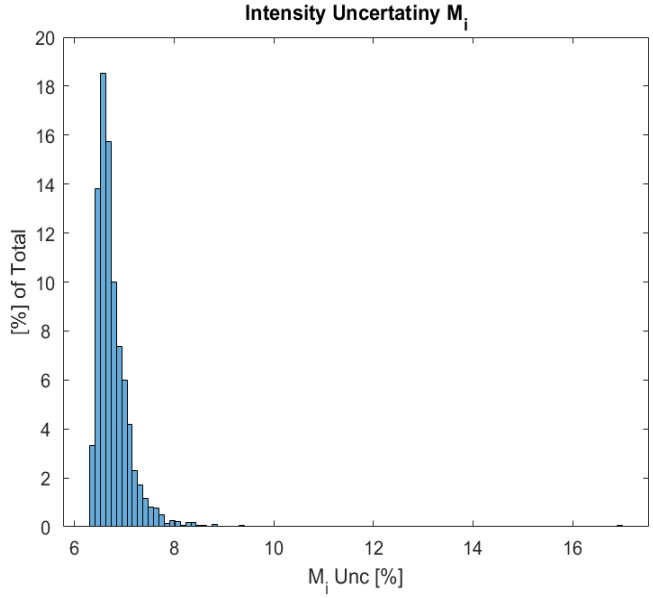

Figure 3.18: Histogram of the uncertainty of the Mach number as a percentage of the total number of data points.

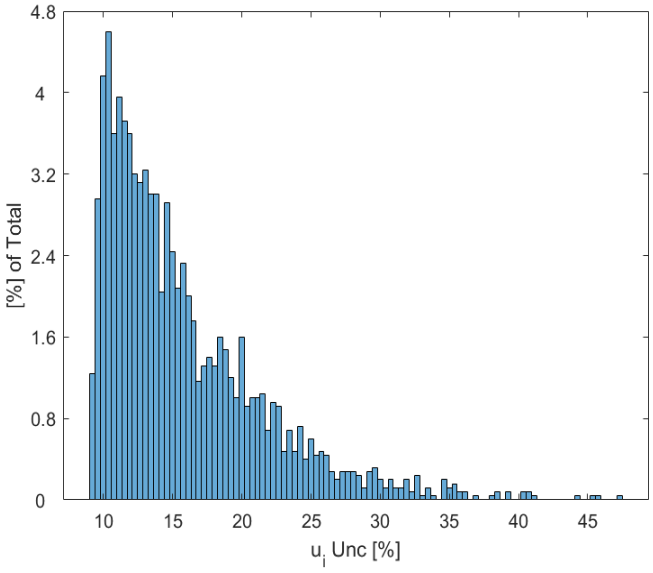

Figure 3.19: Histogram of the uncentainty of the ion velocity as a percentage of the total number of data points.

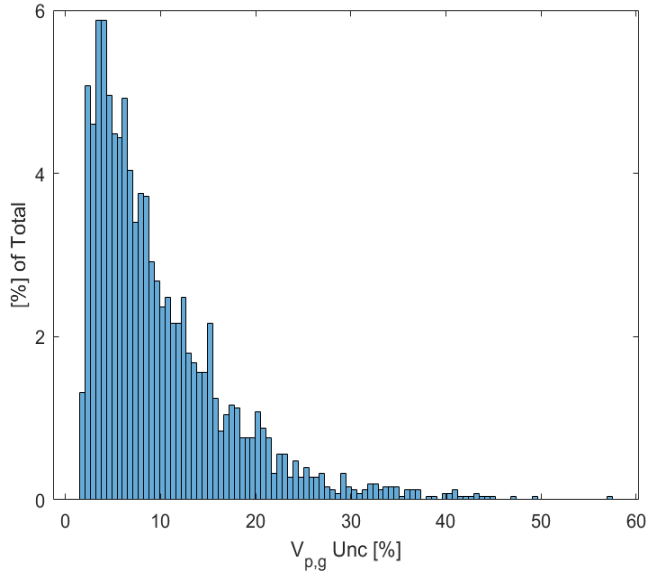

Figure 3.20: Histogram of the uncertainty of the plasma potential relative to ground as a percentage of the total number of data points.

average analytical uncertainty of the electron density was ±5% which was less than the uncertainty for a sheath in the transitional regime, which was ±15% [5]. The total uncertainty for the electron density was ±20%.

The Mach number uncertainty was calculated solely from the uncertainty of the current ratio. The average analytical uncertainty was found to be ±7%. The uncertainty of the ion velocity was calculated based on the calculated uncertainties of the electron temperature and Mach number. The average uncertainty for the ion speed was ±16%. The calculated uncertainty for the plasma potential was ±10%. These uncertainties for electron temperature, Mach number, ion speed, and plasma potential were in line with literature [4, 1, 2]. The electron density uncertainty was found to be less than what appears in literature. In literature the uncertainty for the electron density was on the order of ±50% to ±60% [4, 1].

Chapter 4
CONCLUSION

Results for initial QLP testing have been presented for a 500 W Hall thruster. The QLP was positioned on a dual axis translation stage and on the Hall thruster centerline. The position of the probe was about 6 thruster diameters away from the exit plane of the Hall thruster. At a single Hall thruster operating condition, a breathing mode with a frequency of 28.4 kHz was measured by the graphite electrodes. For this breathing mode the electron temperature and density varied between 1.0-3.4 eV and 0.1-3 $\times$ 10^{17} m^{-3}, respectively. Based on these results the plume conditions did not satisfy ideal thin-sheath Langmuir probe theory. However, these conditions did satisfy the collisionless and end effect assumptions. The sheath thickness could be reduced by lowering the potential difference between probes 3 and 4. The original setting of 26.89 V was based on the maximum potential differences for estimating the sheath thickness in literature [8, 33]. From literature, potentials applied to probes 3 and 4 can be as low as 10 V [5].

The average ion Mach number and velocity were calculated to be 10.9 and 14 km/s, respectively. Measurement error in the collected current of probe 3 was from a sign change in the collected current due to noise. The current ratio between the perpendicular and parallel probe could not be determined accurately. Thus, Mach numbers were calculated to be far greater than 20 which was unlikely based on results from the literature, which had a maximum Mach number of 6 measured from a 5 J pulse for a PPT [33]. The plasma potential was found to vary nominally from 11 V to 22 V relative to ground. When compared with the potential applied to probe 1, it was shown that the applied potential did not exceed the

plasma potential. This confirms standard QLP operation occurred.

Some recommendations for ideal QLP operation are provided. These are recommendations based on experience during data collection and analysis. For more accurate QLP measurements systematic noise in the circuit should be removed. This was the main reason for the positive ion saturation current that was collected from probe 3. Moreover, most of the collected QLP data was not synchronized across oscilloscopes. A pulse or function generator should have been used to synchronize the oscilloscope measurements instead of floating voltage. Also, a lower potential should have been applied to probes 3 and 4 to reduce their sheath thickness. This may allow the use of ideal Langmuir probe theory, but based on the measured values of electron temperature and density, it is probable that this will not be the case. While all QLPs cannot reproduce the same spatial resolution of single Langmuir probes, the spacing between the electrodes could be reduced by half. However, based on this design which utilizes removable graphite probe tips, reducing the spacing between probes may increase the difficulty of installing new electrodes.

4.1 Future Work

Some additional recommendations for future work involving QLPs are based on knowledge of theory and experience with data collection. Apply single Langmuir probe theory in magnetic fields to QLPs. While the magnetic field will be non-uniform over the length of the probe tips or between probes, this could expand the capability of QLPs by making measurements closer to a Hall thruster channel exit if the topology of the magnetic field has been mapped. While the breathing mode may be the most prevalent instability in the Hall thruster plume, a QLP might be able to measure other Hall thruster plume transients that occur near the acceleration channel or cathode. Expand the current measurement resolution

[33]. Especially for this QLP which was larger in radius and length than previous QLPs. By expanding the resolution of the measured current, smaller electron densities can be measured.

BIBLIOGRAPHY

[1] Brian E. Beal. Preliminary plume characterization of a low-power hall thruster cluster. *AIAA 38th Joint Propulsion Conference*, pages 1–16, 2002.

[2] Brian E. Beal. Plasma properties downstream of a low-powered hall thruster. *Phys. Plasma*, 12(123503):1–8, 2005.

[3] Brian E. Beal Beal. Plasma properties in the plume of a hall thruster cluster. *Propulsion and Power*, 20(6):985–991, 2004.

[4] Scott A. Bufton. Exit plane plasma measurements of low-power hydrazine arcjet. pages 1–193, 1996.

[5] Rodney L. Burton. Application of a quadruple probe technique to mpd thruster plume measurements. *Propulsion and Power*, 9(5):771–777, 1993.

[6] Sin-Li Chen and T. Sekiguchi. Instantaneous direct display system of plasma parameters by means of triple probe. *Applied Physics*, 36(8):2363–2375, 1965.

[7] Robert. Eckman. Triple langmuir probe measurements in the plume of a pulsed plasma thruster. *Propulsion and Power*, 17(4):762–771, 2001.

[8] Nikolaos A. Gatsonis. Characterization of a pulsed plasma thruster plume using a quadruple langmuir probe method. *AIAA Propulsion Conference*, 38:1–15, 2002.

[9] Nikolaos A. Gatsonis. Current-mode triple and quadruple langmuir probe methods with applications to flowing pulsed plasmas. *IEEE transactions on plasma science*, 32(5):2118–2129, 2004.

[10] Saravia M. M. Giannetti, V. and T. Andreussi. Measurement of breathing mode oscillation in hall thruster plasma with a fast-diving triple langmuir probe. *Phys. Plasma*, 27(123502):1–14, 2020.

[11] R. J. Goldston and P.H. Rutherford. *Introduction to Plasma Physics*. Taylor and Francis Group, NY, 2000.

[12] James M. Haas. Development of a high-speed, reciprocating electrostatic probe system for hall thruster interrogation. *Review of Scientific Instruments*, 71(11):4131–4138, 2000.

[13] I. H. Hutchinson. *Principle of Plasma Diagnostics*. Cambridge University Press, NY, 2nd edition, 2002.

[14] Robert Jankovsky. High power hall thrusters. *AIAA 35th Joint Propulsion Conference*, pages 1–13, 1999.

[15] Billy H. Johnson and David L. Murphree. Plasma velocity determination by electrostatic probes. *AIAA*, 7(10):2028–2030, 1969.

[16] Michael E. Jones. A grid-based coulomb collision model for pic codes. *Computational Physics*, 123(1):169–181, 1996.

[17] Madhoo Kanal. Theory of current collection of moving cylindrical probes. *Applied Physics*, 35(6):1697–1703, 1964.

[18] Syri J. Koelfgen. Magnetic and langmuir probe measurements on the plasmoid thruster experiment. *AIAA Propulsion Conference*, 40:1–11, 2004.

[19] Christophe Koppel. The smart-1 hall effect thruster around the moon: In flight experience. *29th International Electric Propulsion Conference*, pages 1–9, 2005.

[20] Pascal Chabert Lafleur, T. and Anne Bourdon. The origin of the breathing mode in hall thrusters and its stabilization. *Applied Physics*, 130(5), 2021.

[21] James Laframboise. Theory of cylindrical and spherical langmuir probes in a collisionless plasma at rest. *Rarefied Gas Dynamics*, 2(4):22–44, 1964.

[22] Zhongmin Li. Experimental study of a hall current plasma accelerator. pages 1–117, 2003.

[23] Robert B. Lobbia. Recommended practice for use of langmuir probes in electric propulsion testing. *Propulsion and Power*, 33(3):566–581, 2017.

[24] D.P. Mishra. *Fundamentrals of Rocket Propulsion*. Taylor & Francis Group, LLC, FL, 2017.

[25] M. Mitchner and C. H. Kruger, Jr. Partially ionized gases.

[26] A. I. Morozov. The conceptual development of sationary plasma thrusters. *Plasma Physics Reports*, 29(3):235–250, 2003.

[27] H. M. Mott-Smith and Irving Langmuir. The theory of collectors in gaseous discharges. *Physical Review*, 28:727–763, 1926.

[28] G. Poissant and M. Dudeck. Velocity profiles in a rarefied argon plasma stream by crossed electrostatic probes. *Applied Phyiscs*, 58(5):1772–1779, 1985.

[29] Anna J. Sheppard. Theoretical and experimental performance of an electron cyclotron resonance thruster operating on water vapor propellant. *Diss. University of Washington*, 2021.

[30] George P. Sutton. *Rocket Propulsion Elements*. John Wiley & Sons, Inc., NJ, 9th edition, 2017.

[31] Peter Thoreau and Justin Little. Influence of field topology on magnetically shielded hall thruster performance. *IEPC Conference Paper*, pages 1–15, 2022.

[32] Peter Thoreau and Justin Little. Influence of field topology on magnetically shielded hall thruster plume divergence. *IEEE Conference Paper*, pages 1–8, 2022.

[33] Jurg C. Zwahlen. Investigation of a pulsed plasma thruster plume using a quadruple langmuir probe technique. pages 1–71, 2002.